APPENDIX E

NFCSC DOCUMENT COVER SHEET[1]

Name/Title of Deliverable/Milestone/Revision No. Progress Report on Fuel/Basket Degradation and Waste Package Pressure Effects Modeling

Work Package Title and Number Multiphysics Simulation of DPC Criticality – SNL (SF-20SN01030507)

Work Package WBS Number WBS 1.08.01.03.05

Responsible Work Package Manager Ernest Hardin (Name/Signature)

Date Submitted

Quality Rigor Level for Deliverable/Milestone[2]	☐ QRL-1 ☐ Nuclear Data	☐ QRL-2	☐ QRL-3	☒ QRL-4 Lab QA Program[3]

This deliverable was prepared in accordance with Sandia National Laboratories *(Participant/National Laboratory Name)*

QA program which meets the requirements of

☒ DOE Order 414.1 ☐ NQA-1 ☐ Other

This Deliverable was subjected to:

☒ Technical Review ☐ Peer Review

Technical Review (TR)
Review Documentation Provided

☐ Signed TR Report or,
☐ Signed TR Concurrence Sheet or,
☒ Signature of TR Reviewer(s) below

Peer Review (PR)
Review Documentation Provided

☐ Signed PR Report or,
☐ Signed PR Concurrence Sheet or,
☐ Signature of PR Reviewer(s) below

Name and Signature of Reviewers

Michael Nole/SNL — Michael Nole

Philip Jones/SNL (see other sheet)

NOTE 1: *Appendix E should be filled out and submitted with the deliverable. Or, if the PICS:NE system permits, completely enter all applicable information in the PICS:NE Deliverable Form. The requirement is to ensure that all applicable information is entered either in the PICS:NE system or by using the NFCSC Document Cover Sheet.*

- *In some cases there may be a milestone where an item is being fabricated, maintenance is being performed on a facility, or a document is being issued through a formal document control process where it specifically calls out a formal review of the document. In these cases, documentation (e.g., inspection report, maintenance request, work planning package documentation or the documented review of the issued document through the document control process) of the completion of the activity, along with the Document Cover Sheet, is sufficient to demonstrate achieving the milestone.*

NOTE 2: *If QRL 1, 2, or 3 is not assigned, then the QRL 4 box must be checked, and the work is understood to be performed using laboratory QA requirements. This includes any deliverable developed in conformance with the respective National Laboratory / Participant, DOE or NNSA-approved QA Program.*

NOTE 3: *If the lab has an NQA-1 program and the work to be conducted requires an NQA-1 program, then the QRL-1 box must be checked in the work Package and on the Appendix E cover sheet and the work must be performed in accordance with the Lab's NQA-1 program. The QRL-4 box should not be checked.*

APPENDIX E

NFCSC DOCUMENT COVER SHEET[1]

Name/Title of Deliverable/Milestone/Revision No. Progress Report on Fuel/Basket Degradation and Waste Package Pressure Effects Modeling

Work Package Title and Number Multiphysics Simulation of DPC Criticality – SNL (SF-20SN01030507)

Work Package WBS Number WBS 1.08.01.03.05

Responsible Work Package Manager Ernest Hardin (Name/Signature)

Date Submitted

Quality Rigor Level for Deliverable/Milestone[2]	☐ QRL-1 ☐ Nuclear Data	☐ QRL-2	☐ QRL-3	☒ QRL-4 Lab QA Program[3]

This deliverable was prepared in accordance with Sandia National Laboratories
(Participant/National Laboratory Name)

QA program which meets the requirements of

☒ DOE Order 414.1 ☐ NQA-1 ☐ Other

This Deliverable was subjected to:

☒ Technical Review ☐ Peer Review

Technical Review (TR)
Review Documentation Provided

☐ Signed TR Report or,
☐ Signed TR Concurrence Sheet or,
☒ Signature of TR Reviewer(s) below

Peer Review (PR)
Review Documentation Provided

☐ Signed PR Report or,
☐ Signed PR Concurrence Sheet or,
☐ Signature of PR Reviewer(s) below

Name and Signature of Reviewers

Michael Nole/SNL (see other sheet)

Philip Jones/SNL

NOTE 1: *Appendix E should be filled out and submitted with the deliverable. Or, if the PICS:NE system permits, completely enter all applicable information in the PICS:NE Deliverable Form. The requirement is to ensure that all applicable information is entered either in the PICS:NE system or by using the NFCSC Document Cover Sheet.*

- *In some cases there may be a milestone where an item is being fabricated, maintenance is being performed on a facility, or a document is being issued through a formal document control process where it specifically calls out a formal review of the document. In these cases, documentation (e.g., inspection report, maintenance request, work planning package documentation or the documented review of the issued document through the document control process) of the completion of the activity, along with the Document Cover Sheet, is sufficient to demonstrate achieving the milestone.*

NOTE 2: *If QRL 1, 2, or 3 is not assigned, then the QRL 4 box must be checked, and the work is understood to be performed using laboratory QA requirements. This includes any deliverable developed in conformance with the respective National Laboratory / Participant, DOE or NNSA-approved QA Program.*

NOTE 3: *If the lab has an NQA-1 program and the work to be conducted requires an NQA-1 program, then the QRL-1 box must be checked in the work Package and on the Appendix E cover sheet and the work must be performed in accordance with the Lab's NQA-1 program. The QRL-4 box should not be checked.*

Progress Report on Fuel/Basket Degradation and Waste Package Pressure Effects Modeling

Spent Fuel and Waste Disposition

Prepared for
US Department of Energy
Spent Fuel and Waste Science and Technology
by
Itasca Consulting Group, Inc., and
Sandia National Laboratories, Albuquerque, NM

M2SF-20SN010305073 Rev. 1
January 2021

Revision History

Deliverable: M2SF-20SN010305073 *Progress Report on Fuel/Basket Degradation and Waste Package Pressure Effects Modeling* (Rev. 0) Work Package: SF-20SN01030507 Multi-Physics Simulation of DPC Criticality - SNL WBS: 1.08.01.03.05 Direct Disposal of Dual Purpose Canisters	Prepared at Sandia, with technical reviews by Michael Nole and Philip Jones, compliant with NFCSC/ SFWD QAPD Rev. 6, Appendix B. The Sandia review & approval (Tracking # 1184592) was for internal use only, and the resulting Rev. 0 was submitted to PICS/NE in satisfaction of the deliverable, and to DOE for management review before finalization and publication. The cover sheets attached to the beginning of this document represent the status at deliverable submittal.
Deliverable: M2SF-20SN010305073 *Progress Report on Fuel/Basket Degradation and Waste Package Pressure Effects Modeling* (Rev. 1)	Revision 1 has editorial fixes requested by the DOE reviewer (Figure 2-4 inversion and Table 4-3 caption). Technical reviews for Rev. 0 (see cover sheets) were not repeated. Submitted for Sandia formal review & approval (SAND***-***).

Sandia National Laboratories is a multimission laboratory managed and operated by National Technology and Engineering Solutions of Sandia LLC, a wholly owned subsidiary of Honeywell International Inc. for the U.S. Department of Energy's National Nuclear Security Administration under contract DE-NA0003525.

Sandia National Laboratories

U.S. DEPARTMENT OF ENERGY

National Nuclear Security Administration

Approved for Unclassified, Unlimited Release

Disclaimer

This report does not take into account contractual limitations or obligations under the Standard Contract for Disposal of Spent Nuclear Fuel and/or High-Level Radioactive Waste (Standard Contract) (10 CFR Part 961). For example, under the provisions of the Standard Contract, spent nuclear fuel in multi-assembly canisters is not an acceptable waste form, absent a mutually agreed to contract amendment.

To the extent discussions or recommendations in this report conflict with the provisions of the Standard Contract, the Standard Contract governs the obligations of the parties, and this report in no manner supersedes, overrides, or amends the Standard Contract.

This report reflects technical work which could support future decision making by DOE. No inferences should be drawn from this report regarding future actions by DOE, which are limited both by the terms of the Standard Contract and Congressional appropriations for the Department to fulfill its obligations under the Nuclear Waste Policy Act including licensing and construction of a spent nuclear fuel repository.

Executive Summary

Progress is reported on development and testing of the Fuel/Basket Degradation Model, and the Waste Package Breach Model. The work follows on reported FY19 model development (SNL-ICG 2019).

Modeling has addressed questions framed in the deliverable description: 1) how fuel/basket damage, including from seismic ground motion, could impact reactivity; 2) whether dynamic degradation processes (e.g., caused by seismic ground motion) should be targets for further model development; and 3) what are the key model parameters and how do they affect the likelihood and energy of criticality events.

For basket structure made from aluminum-based metal-matrix composite material, basket collapse would coincide with loss of neutron absorbers, and would occur within a few hundred years after waste package breach. Degradation models discussed in this report have thus far focused on a generic 32-PWR (pressurized water reactor fuel) basket with aluminum-based plates.

Fuel/Basket Degradation Model – The performance of this model was accelerated by porting to the Particle Flow Code (*PFC* 6.0), and implementing special features of *PFC*. The ported model has reproduced earlier results that thinned basket plates will buckle, leading to basket collapse, whereupon the spacer grids will bear the weight of the fuel stack. This condition corresponds to the basket degradation case for reactivity analysis (Clarity et al. 2019), although additional voiding between assemblies may occur because of fuel assembly rearrangement (especially in response to seismic ground motion). Basket collapse is an important transition when fuel weight is transferred from the basket structure to the spacer grids. Timing of the transition depends on rates of corrosion, basket configuration, and modes of deformation.

Basket structure made from stainless steel may not collapse during the period of regulatory concern. The mechanical lifetime of stainless steel (due to corrosion) could be well beyond 100,000 years depending on the thermochemical environment, thereby simplifying reactivity modeling for as-loaded dual-purpose canisters (DPCs). Note that this is for general corrosion, which is relevant if localized corrosion (cracking, pitting) is not the cause of basket collapse. Zircaloy spacer grids and fuel rods corrode very slowly in water, and under the same conditions would also likely have mechanical lifetimes that exceed the period of regulatory concern.

Further degradation beyond basket collapse would involve failure of Zircaloy spacer grids and fuel rod cladding, and is not incorporated in the as-loaded reactivity analysis cases (loss-of-absorber, and basket degradation; Clarity et al. 2019). Using the 2.5-dimensional model, preliminary example calculations show effects from successive spacer grid failures in a sequence of quasi-steady degraded states (Figures 2-8 through 2-10). Rapid deformation of a similar nature could occur with seismic ground motion (which becomes more likely in tectonically active settings as the duration of the time period of interest increases). These results also show that PWR assembly guide tubes (in which disposal control rods could be placed) move with the fuel rods during degradation, as expected. Further reactivity analysis will be helpful for specifying the number and distribution of disposal control rods, re-channeled boiling water reactor (BWR) fuel assemblies, or chevron insert plates (SNL 2020). Coupling of degradation models described here with neutronics and thermal-hydraulics will initially be external, by providing degraded configurations for reactivity analysis.

Planned improvements to the Fuel/Basket Degradation Model include: better discretization of spacer grids and addition of a hinge formation model, and analysis of additional scenarios including failure of the internal DPC basket supports. Recommended additional future work includes: testing the 3-D model, direct simulation of spacer grid collapse from seismic ground motion, tube-and-plate basket structure degradation, further evaluation of the mechanical lifetime for stainless steel basket structures, and simulation of the degraded configurations for criticality control features, particularly re-channeled BWR fuel assemblies and chevron inserts.

Waste Package Breach Model – This model has been expanded in scope from the previous year. Processes added (in addition to fracture growth and canister yielding) include: a zero-dimensional thermal-hydraulic model, heat pulse input, fracture opening/growth in response to pressure produced by heating, venting of fluid pressure, and dissipation of pressure outside the waste package. Multiple successive heating events were simulated, subject to certain model limitations.

A minimum thermal event energy representing a transient criticality event is needed to cause fracture growth or yielding of the canister (approximately 0.2 GJ). At lower energy than this, heat would be absorbed into the canister internals, including water, without producing sufficient pressure to open a fracture or yield the canister shell. Trial model solutions suggest also that there is an energy level greater than 1 GJ and less than 10 GJ at which boiling may occur. The specific conditions for boiling are likely to depend on the rate of heating, localization of heating and transient boiling inside the canister, and the transmissivity of the vessel breach.

Under the assumptions of the model the fracture always opens and grows when a critical pressure is reached. Successive events increase the fracture length, which increases stress concentration around the fracture tips and allows the fracture to open and expel fluid at lower pressures.

In the current model the canister always returns to its original dimensions and the fracture closes at the end of each event. If permanent non-reversible deformation of the canister were included, the fracture could acquire a permanent opening aperture. This could further lower the pressure that could be achieved by subsequent events, which in turn could lower the energy of subsequent criticality excursions because of quicker voiding.

To verify whether and how the spatial and time scales of thermal-hydraulic response could affect criticality event dynamics, will require close-coupling with a neutronic model in future work.

Planned improvements to the Waste Package Breach Model include: incorporating an equation-of-state approach to represent two-phase (water-steam) behavior, and more realistic coupling of backfill pore pressure (external to the waste package) with the in-package thermal-hydraulic model, including conductive heat dissipation. Recommended additional future work includes: evaluating inertial effects on breach opening (which is currently represented by quasi-steady states); evaluating nonlinear plastic behavior of canister/overpack materials; localization of heating inside the canister to represent spatial gradients of pressure and temperature that may exist for short times; and including two-phase cooling and return flow processes that will be needed for coupling with neutronic/thermal-hydraulic models. Notwithstanding these potential improvements, the Waste Package Breach Model has captured key physical processes, and is ready to be used in probabilistic analysis or parametric studies.

Fuel Assembly Cell Model – Previous results from this model are summarized briefly in this report, but further work was deferred for future consideration. The model showed that corrosion products containing absorber material would accumulate in a layer at the bottom of each cell

(containing a fuel assembly). Prior to basket collapse the neutron absorber density would become depleted on the vertical plates, which may increase overall reactivity. This effect is bounded by the loss-of-absorber case that is in use for reactivity analysis (Clarity et al. 2019).

DPC Crush Model – Development of the new DPC Crush Model was in the planning stage when this report was prepared. A technical plan is presented here, for a calculation to determine if ground water pressure or buffer clay swelling pressure could buckle the shell of a DPC (after breach of the overpack but before flooding of the DPC).

Acknowledgments

Author	Organization	Responsible for Sections
Branko Damjanac	Itasca Consulting Group	All
Varun	Itasca Consulting Group	Sections 2 and 6
Jason Furtney	Itasca Consulting Group	Sections 3 and 6
Zorica Radakovic-Guzina	Itasca Consulting Group	Section 4
Michael Nole	Sandia National Laboratories	Reviewer
Philip Jones	Sandia National Laboratories	Reviewer
Ernest Hardin	Sandia National Laboratories	All (SNL Project Lead and Editor)

Table of Contents

List of Figures

List of Tables

Acronyms

2-D	Two-dimensional
2.5-D	Two-and-a-half dimensional (see text)
3-D	Three-dimensional
3DEC	3-D Distinct-element Code
ANA	Advanced Neutron Absorbing material
BWR	Boiling Water Reactor
DPC	Dual-Purpose Canister
EoS	Equation of State
FLAC3D	Fast Langrangian Analysis of Continua in 3-D (simulation code)
FY	Fiscal year
LEFM	Linear Elastic Fracture Mechanics
MMC	Metal-Matrix Composite material
PFC	Particle Flow Code
PGV	Peak Ground Velocity (seismic)
PWR	Pressurized Water Reactor
SCC	Stress Corrosion Cracking
SG	Spacer Grid
SNF	Spent Nuclear Fuel

Progress Report on Fuel/Basket Degradation and Waste Package Pressure Effects Modeling

1. Introduction

This report presents progress on development and testing of dual-purpose canister (DPC) degradation models, in support of postclosure in-package nuclear criticality investigations. The two models emphasized in this report are:

- **Fuel/Basket Degradation Model** – Simulates disaggregation and collapse of the fuel basket and fuel assemblies, due to weakening by corrosion, and shaking by seismic ground motion.
- **Waste Package Breach Model** – Simulates injection of a heat pulse representing a transient criticality event, into a breached, flooded DPC. The breach is represented as a fracture initiated by corrosion, that opens and grows in response to internal pressure.

In addition a modeling plan is presented for the DPC Crush Model, for which development is underway. This report follows on reported FY19 model development (SNL-ICG 2019). Another model, the Fuel Assembly Cell model was reported in FY19 and is briefly summarized here, but further development was deferred.

Development and implementation of the Fuel/Basket Degradation Model and the Waste Package Breach Model has the overall objective to support investigations of postclosure criticality, which may result in criticality control strategies or analysis of criticality consequences. This is conceived as a multi-year investigation that proceeds in stages:

I. **Preliminary** – Model scoping and development, focusing on how degradation processes can be generalized and simplified (determine what is important to predicting configurations). Trends in the evolution of fuel/basket degradation are studied and used to design further stages of investigation. Coupling relationships start simple (one-way) and are expanded to include more complex behaviors (two-way).

II. **Configurations for Reactivity Analysis** – When model development has stabilized to a degree that has reasonable complexity and defensibility, with prospects for validation, then degraded configurations can be selected for reactivity analysis.

III. **Incorporate Fuel/Basket Modifications into Configurations for Analysis** – Fuel/basket modifications (control features; SNL 2020) implemented during loading of future DPCs, would be designed to prevent or limit postclosure criticality of degraded states (SNL 2020). Models of fuel/basket degradation that include these control features could eventually serve in regulatory analysis for licensing of the modifications.

IV. **External Coupling With Other Models (TH, neutronic)** – Progressive states of fuel/basket degradation can be handed off for reactivity analysis by complex criticality event simulation models being developed in parallel.

Model development is currently in Stage I (Preliminary) in which model features and capabilities are being developed and evaluated. This work began at the start of FY19 (Section 1.2), and is planned to continue in FY21, whereupon a summary deliverable of Stage I will be prepared.

This progress report builds on, summarizes, and incorporates information provided in the FY19 report (SNL-ICG 2019). The modeling approach focuses on the unique capabilities of the simulation code set available from Itasca Consulting Group, Inc. including the *FLAC3D*, *3DEC*, and *PFC* codes. *FLAC3D* is a continuum mechanics code with features such as structural elements and defined interfaces, that can be used to represent complex deformation of structures such as DPC shells and baskets. *3DEC* is a distinct-element modeling framework that defines discrete bodies (e.g., fuel rods, nozzles, etc.) which interact and can detach and fall when damaged. *3DEC* blocks can also simulate continuum behavior. *PFC* implements a generalization of the distinct-element method in which all bodies are spheres or polyhedra of variable size, that can be attached to represent more complex shapes, or even continuum behavior. In the distinct-element method bodies can be joined, or interact with each other in a general way, resulting in potential detachment and falling under gravity, forming new assemblies (accumulation of loose particles). All three of these codes implement rigorous inertial force balances, and therefore can be "shaken" to represent the effect from seismic ground motion. Also, the codes are operated using a scripting language with many common features, so that code features such as constitutive relations, runtime commands, input/output, graphics, etc. are shared.

The work described in this report is part of a multi-year R&D effort to be undertaken in parallel with related investigations of postclosure criticality (Section 1.3). It describes the second year of an investigation begun in FY19 (SNL-ICG 2019). Much of the work so far has been performed by Itasca Consulting Group under Sandia Purchase Orders: #2073207 Rev. 6 (June 8, 2020), #2073207 Rev. 2 (October 31, 2019), #2073207 Rev. 0 (August 6, 2019), #2019960 Rev. 0 (March 21, 2019) and #1978922 Rev. 0 (October 26, 2018).

1.1 Modeling Background

The previous report (SNL-ICG 2019) led with a literature review of cladding and fuel/basket material degradation processes, which include:

- **Initially failed cladding** – An uncertain fraction of fuel has pinhole penetrations or fine cracks, which may be undetected. These could be the sites for progressive degradation of fuel rods.
- **Cladding creep rupture** – Could be an important degradation mechanism for fuel rods but only if waste package temperatures are elevated (e.g., by quasi-steady criticality).
- **Axial clad splitting at unsaturated, oxidizing conditions** – Progressive failure of the cladding on individual fuel rods can occur in the presence of moisture and air, at elevated temperatures. An initial penetration flaw is needed to initiate the splitting process. Splitting is apparently unlikely at saturated, chemically reducing conditions such as would occur within breached waste packages, in repository settings below the water table.
- **Zircaloy corrosion mechanisms** – Corrosion of fuel cladding or spacer grids can proceed by various mechanisms including general corrosion, localized corrosion, and stress corrosion cracking. Zircaloy is highly resistant to corrosion so concentrated and aggressive aqueous conditions are required (such as might occur from evaporative concentration in unsaturated repository settings).
- **Corrosion of basket materials** – Baskets are nearly all made from stainless steel, or aluminum-based metal-matrix composite (MMC) materials (e.g., Metamic-HT®). General corrosion could lead to failure of aluminum-based basket materials in any repository

setting. For stainless steel, localized corrosion could be important particularly in regions of the basket such as welds and joints between plates, that are subject to greater stresses.

- **Fuel component deformation and failure under load** – Spacer grids, guide tubes (for pressurized water reactor fuel), tie rods (boiling water reactor fuel), end nozzles, and fuel rods are subject to initial stresses acquired during fuel fabrication. During postclosure fuel/basket degradation additional loads can result as the basket structure fails and load is redistributed through fuel assembly spacer grids.

The latter three of these processes, which affect the basket structure and fuel degradation after basket failure, were incorporated in the Fuel/Basket Degradation Model. Parsing of the evolution of fuel/basket degradation into stages is possible using the corrosion lifetime of components (Section 1.2.2). Aluminum-based components would fail first, followed by basket structure if it contains carbon steel or stainless steel, followed by Zircaloy. Fuel cladding degradation by corrosion and mechanical damage is potentially important to criticality analysis but is likely to occur after basket degradation, starting at roughly the same time as spacer grid degradation.

1.2 Previous Model Development

The following discussion summarizes previous model development (SNL-ICG 2019). The reader is referred to that report for details including graphical figures. The DPC Crush Model was not worked on previously (and is currently at the planning stage; Section 4) and so is not described.

1.2.1 Fuel Assembly Cell Model

The Fuel Assembly Cell Model was set up to describe the corrosion of basket plates surrounding a single pressurized water reactor (PWR) fuel assembly, in a generic egg-crate type basket (SNL-ICG 2019). The purpose of the model was to study the release of corrosion-product particles from the plates, which could lead to steady-state criticality. Also, the model can simulate the redistribution of particles in response to seismic ground motion, which could lead to a transient criticality event.

The model domain consisted of a thick slice through a cell, located between spacer grids so that only fuel rods surrounded by water, bounded by basket plates, are in the model. Corrosion generates spherical product particles, which were joined in clumps of two to prevent unconstrained rolling. The clumps were subjected to buoyant forces and Stokes drag during settling. For average particle size of 50 μm, the terminal settling velocity was estimated to be in the range 0.1 m/sec to 0.01 m/sec, depending on the temperature and viscosity of water.

Particle settling was simulated for varying quantities of particles (estimated from the amount of plate corrosion using a relative time measure), and for 0° and 30° inclination of the cell. Particles were uniformly distributed over the bottom of the cell, except that more of them accumulated at the corners because of the guiding effect of the vertical basket plates. Seismic response was simulated using a 3-axis ground motion history used for the Yucca Mountain project (BSC 2004) with 1.05 m/sec peak ground velocity (PGV). Seismic motion caused resuspension of the particle clumps that increased with duration of the event, followed by resettling into a configuration similar to that before the event.

The size of released particles is a factor in settling behavior. More realism could be obtained by modeling the formation and aggregation of corrosion product particles mechanistically. The basket plates could be represented by adherent spherical balls that weaken from corrosion and form corrosion product clumps that are detached and released. Criteria for bonding forces between

particles would be needed to represent corrosion product release and spallation during seismic events. Particles on the roof of the cell could be more readily released than those on the sides. Accounting for particles that are degraded and released would also explicitly represent thinning of the plates. Spatially heterogeneous degradation properties could also improve realism, e.g., representing weld-affected zones, spatially varying temperature, and partially saturated conditions in the canister. Validation data for such criteria could require physical experiments.

For FY20, further work on the Fuel Assembly Cell was deferred in order to make additional resources available for the other models discussed in Sections 2 through 4 below. Eventually the Fuel Assembly Cell Model could be further developed to include: 1) more realistic representation of plates and corrosion products as discussed above; 2) boiling water reactor (BWR) fuel assemblies; and 3) stainless steel basket plates with Boral® sandwich-style absorber plates.

1.2.2 Fuel/Basket Degradation Model

Analysis of basket stability started with a series of studies of basket plate buckling response, then proceeded to a full 3-D model of the basket loaded with fuel. Initially, models accurate at different scales were created to investigate the onset of basket instability and collapse. With the waste package situated horizontally and the basket aligned with the vertical, shearing and bending of the horizontal plates became a relevant failure mechanism with the plate thickness less than 1 mm (reduced by corrosion). However, buckling failure of the vertical plates could occur for thickness of approximately 2 to 2.5 mm if a horizontal gap exists between the basket and its supports. If the canister is more tightly constrained laterally by the supports, then buckling does not occur until vertical plate thickness is 1 to 1.5 mm. At these thickness values the vertical plates belonging to the two lower levels of the basket will buckle under the weight of the fuel.

Buckling involves large displacements, such that basket plates will come in contact with the spacer grids. Spacer grids can thereby constrain buckling within a specific cell, however, as a result the effective span of the horizontal plates increases. Overall, the initial studies for the Fuel/Basket Degradation Model showed that basket collapse due to thinning of the plates will occur from vertical plate buckling when their effective thickness reduces to 1 to 2 mm. Interaction of buckling with plate bending and shearing was not investigated in these studies.

Model development proceeded to 3-D representation of the canister shell, basket, and fuel assemblies including spacer grids and nozzles (Figure 1-1). Two types of models were set up, with the main difference being the level of detail used to represent the fuel assemblies. For the detailed model each fuel rod and guide tube was represented discretely using small blocks, and for the simplified model each fuel assembly was represented by larger blocks with approximately equivalent deformability. The two models were set up using modules for each component so that the level of detail for any component could be changed without affecting the rest of the model. Three types of modules were produced: for fuel assemblies, basket plates, and the canister shell.

The detailed model simulates individual fuel rods and guide tubes (SNL-ICG 2019). Fuel rods were represented by polygonal elements (in cross section) which were connected in *3DEC* (the model has since been ported to *PFC*, a different code, as described in Section 2.1). The rods were modeled as a uniform material with properties based on analysis of cladding and fuel pellet. Fuel rod characteristics were validated using a single-rod model, comparing to experimental flexure data. The model also included discrete spacer grids and end nozzles. Element connections between the blocks representing spacer grids and the fuel rods were defined to allow slip in the axial direction. Element connections between guide tubes and the end nozzles could be adjusted to

represent full bonding or complete separation depending on the state of nozzle damage. Connections between the fuel rods and nozzles initially provided transverse constraint to rod movement, but allowed axial slippage so the rods could pull out completely free of the nozzles. Basket plates and the canister shell were represented using insights from the initial studies discusssed above. The model domain could be adjusted to represent the entire DPC, or only a thick slice perpendicular to the axis, between two adjacent spacer grids (2.5-D model inset in Figure 1-1).

The detailed model was suitable for validation, but a more efficient model with simplified fuel components was developed to reduce run times (e.g., for seismic ground motion simulation). In the simplified model each fuel assembly was replaced by a set of coarsely discretized blocks with equivalent deformability, density, and strength. In other words, equivalent continua were used to represent the rods and spacer grids, with parameter values calculated internally from the material parameters used for the detailed model. The simplified model could be justified by observing from the detailed model that fuel rods bend, but generally do not break when the basket plates and spacer grids are removed.

Simulations proceeded in phases, for both the detailed and simplified models:

- Phase 1: Initial static equilibrium was established under gravity, with all fuel and basket components intact.
- Phase 2: Basket plate corrosion was represented by deleting the basket plates, so that the fuel assemblies stacked on top of each other. The final configuration was controlled by the configuration of internal supports in the canister. (More detail could be added here by successively degrading the basket structure by breaking connections between basket plates based on insights obtained from the *FLAC3D* model.)
- Phase 3: Degradation of spacer grids was represented by removing the grids, and running the model to static equilibrium again. At this stage the nozzles and guide tubes, and the fuel rod cladding, were still intact.

Bending of fuel rods due to gravity was observed in Phase 1. The influence of the lateral basket supports (between the basket and the canister shell) was observed in Phase 2, during which the fuel assemblies fall into a new configuration corresponding to the basket degradation case for criticality studies (Clarity et al. 2019). In Phase 3 the height of fall resulted in rod failures and pulling out of rods from the nozzles. If degradation of the fuel rods is negligible then they behave elastically, and approximation of the final configuration in Phase 3 by the simplified model is realistic.

To further explore the capability of the Fuel/Basket Degradation Model, a seismic study was done in which the simplified model was subjected to a 3-axis ground motion history similar to that discussed for the Fuel Assembly Cell Model but with a stronger, 5.35 m/sec PGV (BSC 2004). Successive configurations of the fuel and basket were generated during the shaking. The results indicate that fuel assemblies are relocated in the stack but remain horizontal and parallel when they come to rest. There is some bending and possible twisting of the fuel assemblies during shaking.

The next steps in development of the Fuel/Basket Degradation Model are described in Section 2.

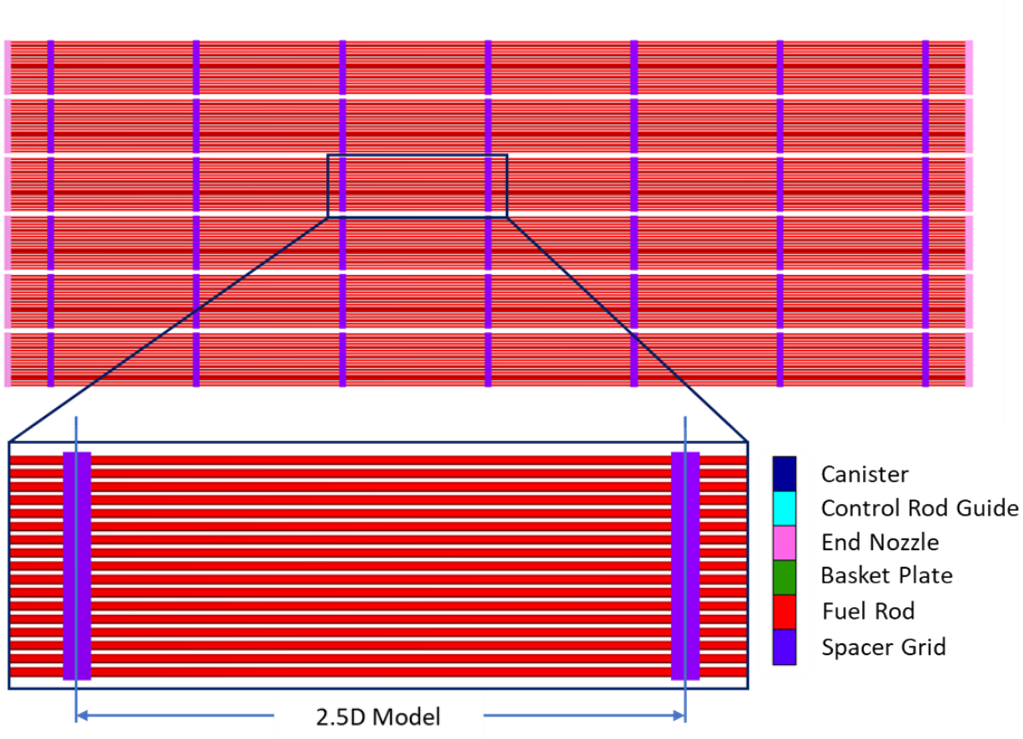

Figure 1-1 Side view of detailed 3-D model, and inset depicting 2.5-D model.

1.2.3 Waste Package Breach Model

This model was developed to investigate the effect of internal pressure such as could result from a criticality event, on a pre-existing breach in the DPC shell or the disposal overpack. The DPC shell and possibly the disposal overpack would be made from stainless steel, or other materials subject to stress corrosion cracking (SCC). Over many thousands of years it is envisioned that the overpack would breach, possibly by cracking, and the DPC shell would breach by cracking at or near welds. This could allow ground water to fill the canister, leading to degradation of neutron-absorbing components so that a criticality event could occur. Such an event would create transient temperature and pressure conditions, and the internal pressure changes could cause initial fractures in the canister and overpack to widen, and possibly to grow. It is important to understand the potential for changes in hydraulic transmissivity between the canister and surroundings because: 1) it could control the potential for, and frequency of, subsequent criticality events; and 2) it could control the release of radionuclides from the canister.

The study used *FLAC3D* to model deformation, yielding, and fracturing of the canister and overpack (SNL-ICG 2019; Itasca 2019). Four 3-D hollow-cylinder model geometries (representing different geometries of the initial fracture breach) were considered: two cases with a longitudinal fracture and two cases with a circumferential or "hoop" fracture. The fractures were oriented perpendicular to the outer surface of the cylinder wall. For each fracture orientation, two fracture locations were considered: one in the middle of the canister and one near the end. For each geometry, three different values of initial fracture length were considered. For each geometry and fracture length, two wall thicknesses were considered: 1.2 cm to represent the DPC shell, and

2.5 cm to represent the overpack (24 cases total). The model was not set up to represent the canister and overpack simultaneously; each component was modeled separately.

A spatially uniform and incrementally increasing pressure was applied to the inner surface of the canister, so the models were quasi-static (neglecting inertial effects from rapid loading, although this could be activated). The model was then solved to equilibrium. The internal canister pressure during an actual criticality event may vary with time due to evolving internal energy and due to mass escaping the package. The analysis considered the limiting case where pressure is constant for long enough to cause fracture growth or other failure in the canister. Once mechanical equilibrium was reached at a given pressure, the pressure was increased, and mechanical equilibrium was reestablished. The model was stopped when the critical pressure (that causes vessel failure by fracture growth or yielding of the cylinder wall) was reached. Initial residual stresses (responsible for development of the initial cracks) were not considered, because residual stresses are localized, and because stresses that cause unstable fracture growth or yielding of the canister wall are greater than residual stresses.

Typical values for properties of stainless steel were selected (SNL-ICG 2019). Yield strength at 200°C in a linearly elastic–perfectly plastic model, was assumed to be 445 MPa reduced by 5% to account for variations in temperature and metal grade. In addition, the mechanical response of stainless steel is not perfectly plastic, so that yield and ultimate strengths generally differ. Therefore, a second set of analyses was performed with a more conservative yield strength value of 300 MPa. The elastoplastic response of steel was represented by the von Misses criterion.

The study assumed that propagation of the initial crack would be Mode I (i.e., opening) and governed by linear elastic fracture mechanics (LEFM). Mode I fracture toughness (K_{IC}) for stainless steel can vary between 40 and 100 MPa-m$^{1/2}$, and a value of 50 MPa-m$^{1/2}$ was used for the canister and overpack. Modeling fracture propagation numerically presents significant challenges and can be computationally intensive. For this study, it was assumed that the fracture propagates along a specified trajectory (i.e., a pre-defined fracture in the model grid). A *FLAC3D* interface along the assumed path of fracture growth was explicitly introduced into the model geometry and was initially bonded to represent unfractured material.

Two failure criteria are possible for both the canister and overpack: fracture propagation and plastic yielding. To accommodate both modes each model is run twice: 1) using an elastic constitutive behavior for the steel and a LEFM criterion for fracture propagation; and 2) an elastoplastic criterion for the steel, without an initial fracture. The model that fails at the lowest pressure is considered the critical mechanism for that configuration (i.e., the actual failure mechanism).

The following observations were made (SNL-ICG 2019):

- Fracture growth did not happen if the ultimate strength of stainless steel was reached before the critical pressure for fracture growth.
- In all cases analyzed the failure processes (both fracturing and yielding) were unstable. Once failure started, it continued at a constant pressure. Note that these models are quasi-static, with constant pressure. This behavior could change in a dynamic model that includes inertial effects and rapid loading.
- For both the canister and overpack thicknesses, longitudinal initial fractures around 1 cm and longer grew due to internal pressurization.

- The critical pressures required to fail the overpack were greater than those for the thinner canister shell.
- For both the canister and overpack, hoop fractures with the assumed initial length less than approximately 6 cm did not grow before plastic yielding of the vessel wall occurred. For fracture length more than approximately 6 cm, failure was controlled by fracture propagation.

The next steps in modeling WP breach behavior are to develop a dynamic pressure-time history using a thermal-hydraulic model for a constrained volume of fluid, adding a pulse of heat to the fluid, and allowing the resulting pressure to open the vessel breach and vent fluid to the external environment. Those developments are described in Section 3.

1.3 Ongoing Related Work

The Fuel/Basket Degradation Model and the Waste Package Breach Model focus on the degraded states of breached packages, and the effect of canister/overpack breaches on criticality event dynamics. The capability to represent these processes is sought for criticality consequence studies (Price et al. 2019) and eventually to support models that couple neutron propagation, thermal-hydraulics, and mechanical processes (Davidson et al. 2019).

1.4 Deliverable Description

The following is paraphrased from the controlling work planning and reporting application (www.picsne.com). This report will summarize progress in FY19-20 on modeling of fuel assembly and DPC basket degradation in the disposal environment, and waste package breach behavior in response to internal heat generation. For preliminary model development, implement one-way coupling between degradation processes and mechanical deformation, and between heat generation (representing criticality) and thermal-hydraulic and mechanical responses of the waste package. Identify key parameters and how they affect the occurrence and energy of criticality events. Assess how fuel/basket damage, including from seismic ground motion, could impact reactivity and whether dynamic degradation processes should be targets for further model development.

2. Progress Report on Fuel/Basket Degradation Model

2.1 Modeling Plan

The purpose of the Fuel/Basket Degradation Model is to study configurations that arise from corrosion and seismic ground motion. Previous work on this model (SNL-ICG 2019) started by using continuum mechanics (*FLAC3D* code) to investigate the mechanical responses of basket plates. This information was then used to represent the basket in the Fuel/Basket Degradation Model (*3DEC* code). In addition, in the *3DEC* model when components degraded (fuel rods, basket plates, and other components) they were retained as disaggregated pieces rather than removing them completely from the model.

In the present continuation of the earlier work, the following features have been, or are planned to be added to the Fuel/Basket Degradation Model:

- Hinge behavior at joints between basket plates, where appropriate and significant to basket stability.
- Spacer grid collapse under load, after degradation of basket plates.
- Displacement of control rod guide tubes as the fuel stack collapses from degradation of basket plates and spacer grids.

As part of this phase, the existing model will be ported from *3DEC* 5.2 (Itasca 2016) to *PFC* 6.0 (Itasca 2018). *PFC* stands for particle flow code, and the latest version supports modeling rigid blocks of any convex shape, with full multi-threading that produces much faster runs on appropriate platforms, compared to *3DEC* where rigid blocks runs are not multi-threaded. *PFC* 6.0 also uses the new command syntax which is consistent among all new versions of Itasca codes and allows easier integration or switching between codes if needed in the future.

Hinge Behavior at Basket Plate Joints – In the model developed previously (SNL-ICG 2019) the basket plates are discretized along length and thickness. This allows them to bend, buckle and break along the length and to bend and break at the joints. Hinge formation at the joints can be added by using a different contact model at the joints. The joints between the vertical and horizontal plates can be weakened to approximate slot-in connections of the basket plates. The parallel bond contact model in *PFC* allows creation of a bond in parallel with the linear contact model. By creating a parallel bond with appropriate tensile strength, using a small value for the radius multiplier and zero moment contribution factor, it is possible to make the joint behave as a hinge with a very small amount of moment resistance (adjustable) after the linear contact has broken, as long as the tensile strength of the parallel bond is not exceeded. A small-scale model with a single cell will be developed first for proof-of-concept.

Spring Forces on Fuel Rods – There are two different types of springs that bear on the fuel rods: the first type are the hold-down springs in the top end nozzles that can induce compressive forces in fuel rods (and tensile forces in guide tubes). These springs apply tractions to fuel rods in the reactor but are not likely to be important after disposal (unless the fuel rods undergo gross axial displacement). The nozzles constrain transverse movement of the rod ends, until such time as the rods pull completely away from the nozzles. The guide tubes will initially be clamped in the nozzles at both ends (by bonding the blocks representing the nozzles and guide tubes using a high cohesion value).

The second type are the springs in spacer grids that keep the fuel rods in place by applying transverse forces from four sides. With four springs per rod for each spacer grid, it would be computationally prohibitive to represent the individual springs. We understand that the compressive forces are required only to calculate the frictional force between spacer grids and fuel rods if the rods try to slide out of the spacer grids. This can be modeled by increasing the thickness of spacer grids in the model so that there is initial overlap between the spacer grid and fuel rods. The overlap generates a compressive force as a function of amount of overlap as shown in Figure 2-1. This method works for both *3DEC* and 3-D *PFC* models. The effective density of spacer grids will need to be adjusted so that the total mass remains the same. A small-scale model with a single fuel rod will be developed first to calibrate the amount of overlap and verify the pullout behavior.

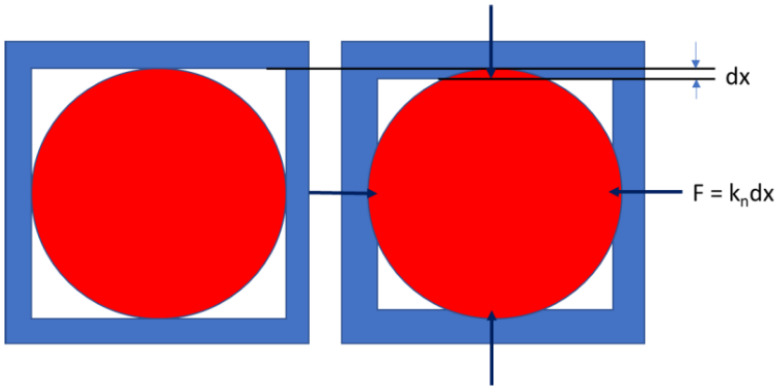

Figure 2-1 Modeling compressive forces on fuel rods.

Degradation of Fuel/Basket Components – The sequence of degradation steps along with approximate timeline for different components is shown below. Note that the degradation times are order-of-magnitude approximations used to set the sequence in which different components degrade.

1) MMC basket plates (mainly aluminum): mechanical lifetime 500 years (based on two-sided corrosion, 1 cm thickness, and rate of 10 μm/year). A more precise projection of basket plate lifetime (e.g., for anodized plates) is not needed for plates that degrade significantly faster than any other fuel/basket component.
2) Stainless steel nozzles: mechanical lifetime 2,500 years (based on two-sided corrosion, 5 mm smallest thickness and 1 μm/year). Blocks of uncorroded steel will likely remain after disintegration of the nozzles, but these will not constrain the fuel or basket.
3) Stainless steel canister and overpack: corrosion lifetime 25,000 years (based on two-sided corrosion, 50 mm thickness and 1 μm/year). Containment lifetime would be substantially less than the corrosion lifetime, and mechanical lifetime (constraining the fuel and basket) would be comparable to corrosion lifetime (order of magnitude). Note that the canister and overpack act together in the model, so they need not be considered separately.

4) Zircaloy spacer grids: corrosion lifetime would be on the order of 500,000 years (based on two-sided corrosion, assumed thickness of 1 mm, and 0.001 μm/year), but mechanical lifetime could be less due to failure under load.

5) Zircaloy fuel cladding: corrosion lifetime would be on the order of 500,000 years (based on one-sided corrosion, assumed intact thickness of 500 μm, and 0.001 μm/year). The failure loading regime would be different from spacer grids, with variation of cladding stress as penetration occurs relieving internal gas pressure, and bending that occurs after spacer grid failure. Mechanical lifetime is assumed for this analysis to be greater than for spacer grids.

6) Zircaloy control rod guide tubes: 500,000 years (based on two-sided corrosion, assumed thickness of 1,000 μm, and 0.001 μm/year). Loading conditions will change as tension is decreased by nozzle failure, then bending that occurs after spacer grid failure.

Based on these estimates the sequence of component failures is described in Section 2.2.3.

The fuel rod cladding and spacer grids are made of similar material with similar thickness. However, once the basket plates collapse, the spacer grids support the weight of the fuel assemblies and will fail under load before degrading completely. Failure of some or all spacer grids would take place before the 500,000-year corrosion lifetime indicated above. Modeling the degradation of spacer grids by discretizing them along the thickness of Zircaloy sheet is infeasible due to the computational effort involved. A different approach will therefore be used whereby the intact spacer grid that is under the greatest load will fail, and more grids will be failed successively using the same criterion, to examine the kinematics of degradation. This will be done once the basket plates and end nozzle connections have failed, but with constraint from the circular envelope of the degraded canister plus the overpack, and prior to failure of fuel rods or guide tubes. It is proposed to allow failure in shear and hinge formation only at the joints making up the spacer grid as shown in Figure 2-2. The approach is an approximation to potentially complex modes of spacer grid failure, and can be revisited in a future study once the successive-failure approach is better understood.

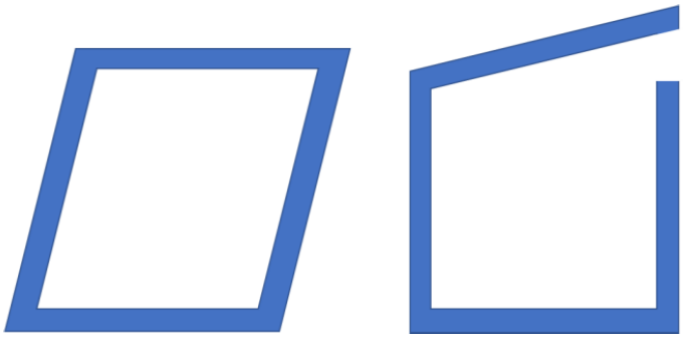

Figure 2-2 Modeling failure of spacer grid using hinge formation (left) and failure at joints (right).

2.2 Summary of Modeling Progress

This section summarizes progress on numerical modeling of fuel/basket collapse in a generic 32-PWR DPC. Over geologic timescales (tens to hundreds of thousands of years) it is envisioned that the disposal overpack and the DPC shell will be breached by initial cracks or fractures due to stress corrosion. A breach in the canister could allow ground water to fill the canister, especially in a saturated-zone repository (but also in an unsaturated repository although the circumstances would differ). Resulting corrosion of the canister internals is likely to degrade the neutron absorbing function, which is provided by various aluminum-based materials for most DPCs of existing designs. Typical ground water acts as a neutron moderator so that criticality could occur.

The purpose of the Fuel/Basket Degradation Model is to simulate evolution of the configuration of basket structural elements and fuel assemblies, falling under gravity within the canister as a result of degradation by corrosion, and seismic ground motion. A generic 32-PWR egg-crate style basket with plates of aluminum-based MMC material was selected for study. During previous work (Section 1.2.2) continuum mechanics (*FLAC3D*) was used to investigate responses of the basket plates, which were then incorporated into a distinct-element model of the basket (*3DEC*). In addition, degraded components (fuel rods, basket plates, and other components) were represented as disaggregated pieces rather than removing them from the model.

For this phase, the following features were proposed to be added to the basket degradation model:

- Porting the model from *3DEC* 5.2 to *PFC* 6.0;
- Representing degradation of spacer grids and nozzles (long corrosion lifetimes except for springs and fasteners); and
- Sensitivity analyses with respect to degradation sequence and effect of randomness.

Any compression of fuel rods by hold-down springs in the end nozzles is deferred at this stage of model development, mainly because the fuel rods would likely be decompressed after disposal, and the springs would be stressed and subject to corrosion. Detailed consideration of the joints between the plates is also deferred, because the spacer grids will stack up anyway after complete failure of the plates. The processes leading to degradation of basket plates is an item of future interest (Section 6.1).

2.2.1 Model Setup and Porting to *PFC* 6.0

The existing detailed Fuel/Basket Degradation Model was ported from *3DEC* 5.2 (Itasca 2016) to *PFC* 6.0 (Itasca 2018). The latest version of the *PFC* code supports modeling rigid blocks of any convex shape and offers the following advantages over *3DEC*:

- Full multi-threading which speeds run time on multi-core machines compared to *3DEC* where rigid blocks runs are not multi-threaded. With this change, simulation of the progressive degradation of a fully detailed 3-D model of a DPC is expected to take 7 to 10 days on an updated Windows workstation.
- Other advanced features useful for this analysis, such as more parameters to describe the contact-detection scheme and the ability to use exact overlap volume to compute contact stiffness, both of which are useful for this particular problem.

- A built-in library of different types of contact models, which can be modified to model additional behavior such as hinge formation, or to model bilinear moment-curvature behavior of fuel rods in a simplified manner with less computational cost.
- *PFC* also uses the new command syntax, which is consistent among all new versions of Itasca codes and allows easier switching between codes in the future if needed.

Similar to *3DEC*, models are templated in *PFC* such that the model developer can specify the geometry and material parameters, and then use scripting language functions to set up and run the model. This model is set up using modules for each component so that the level of detail for any component can be changed without revising other parts of the model. The three such modules are for fuel assemblies, basket plates, and the canister shell.

As described below two types of models have been set up which differ in terms of length along the axis of the canister. The first model, referred to as the 2.5-D model, simulates the length between the centers of two adjacent spacer grids (about 1/7th of the total model in the axial direction), whereas the second model simulates the entire canister, including the end nozzles. The purpose of the 2.5-D model is to test model features and scenarios quickly and gain insight into model behavior before running full-length models with longer run times. Fuel rods, guide tubes, spacer grids, end nozzles, basket plates, and the canister are all modeled individually, similar to the detailed model described previously (Section 1.2.2; also SNL-ICG 2019). The 3-D model in which the entire length of the canister is modeled, is depicted in Figures 1-1, 2-3 and 2-4. Figure 1-1 also shows the modeled length for the 2.5-D model.

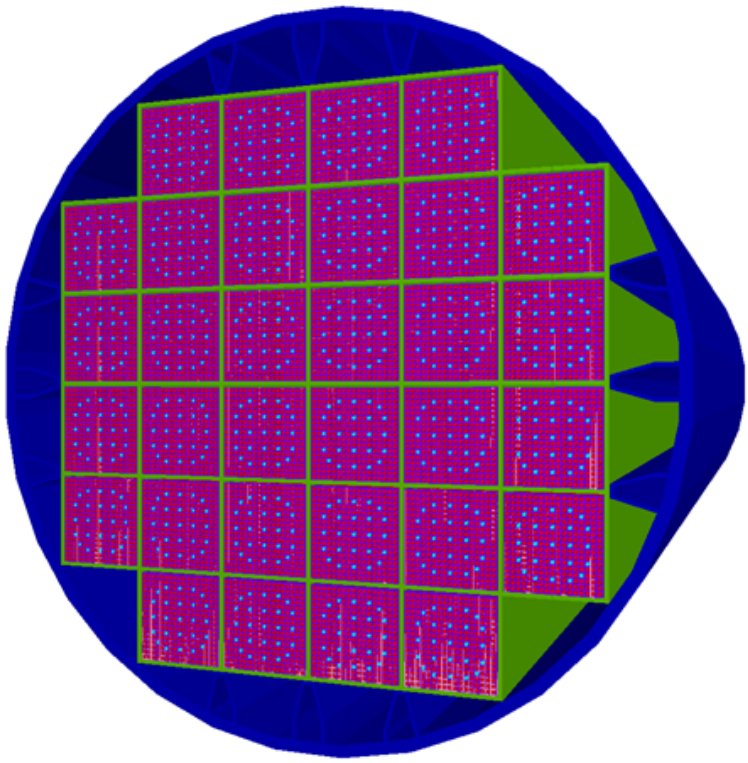

Figure 2-3 Model setup showing components in perspective view.

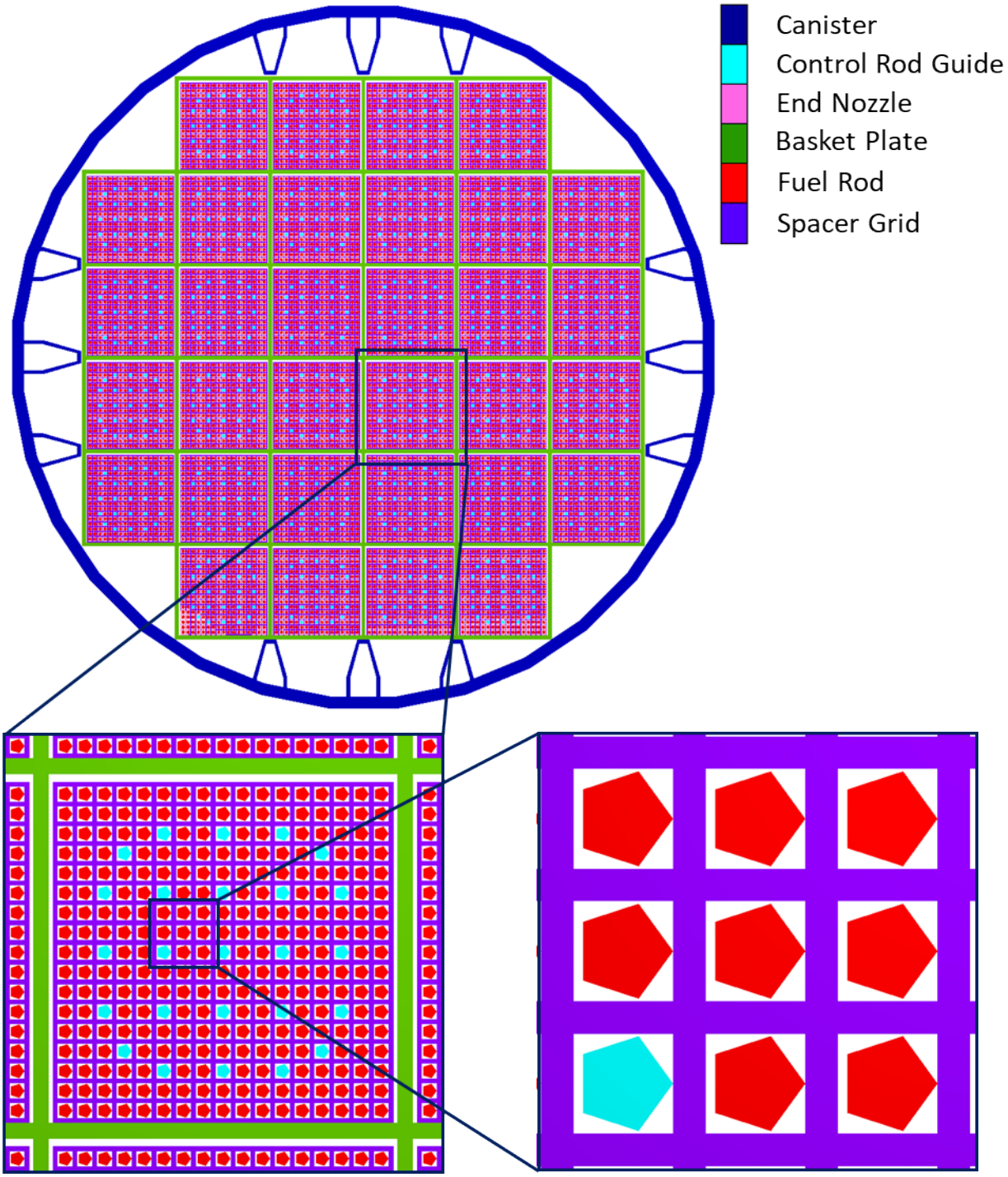

Figure 2-4 Model setup showing components in transverse view.

2.2.2 Single Rod Submodel Implementation in *PFC* 6.0

A single rod model is used to calibrate the bending behavior of a single fuel rod, similar to the approach used for *3DEC* (SNL-ICG 2019). The contact stiffness is proportional to the modulus of the rod and inversely proportional to the segment size because the segments themselves are rigid

and the deformability is concentrated at the contacts. The user only needs to input the modulus and tensile strength of the material, and the contact stiffness and strength are calculated within the model. The fuel rod is loaded in pure flexure by imposing rotation of both ends so that the resulting moment-curvature curve can be compared with laboratory data (Ahn et al. 2018). The rod behaves as a composite beam with spent fuel inside showing brittle behavior and the surrounding zircaloy casing being ductile.

In *3DEC*, a single contact between two segments is composed of multiple sub-contacts. To match the bilinear response observed in the lab, it was assumed that once a sub-contact fails, the tensile strength of the fuel portion decreases to zero (brittle failure) while the casing (ductile failure) provides the residual strength. A length of about 10 cm for each element representing a fuel rod was selected as a compromise between detail and run time, consistent with the available single-rod bending data (SNL-ICG 2019, Section 5.2).

Given the large number of such contacts used to discretize the rods in the 3-D model, the additional computational costs are significant. *PFC* uses a simplified lumped constitutive model at the contact, which reduces that computational cost. Currently, the lumped constitutive model is calibrated to match the secant modulus for the bilinear moment-curvature curve at 2 m^{-1} (Figure 2-5). However, a modified *PFC* modeling feature (*softbond*) is currently being tested. In the modified model, once the maximum tensile stress due to bending reaches a certain value (specified using calibration), the tangent modulus is reduced. Unloading after this point still uses the original modulus, resulting in hysteresis. From preliminary indications this will provide gives a better match with lab results (Figure 2-5) similar to what was obtained using *3DEC* (SNL-ICG 2019, Section 5.2). The quality of fit to the lab data is judged to be adequate for this preliminary model, but might be refined in a future sensitivity study.

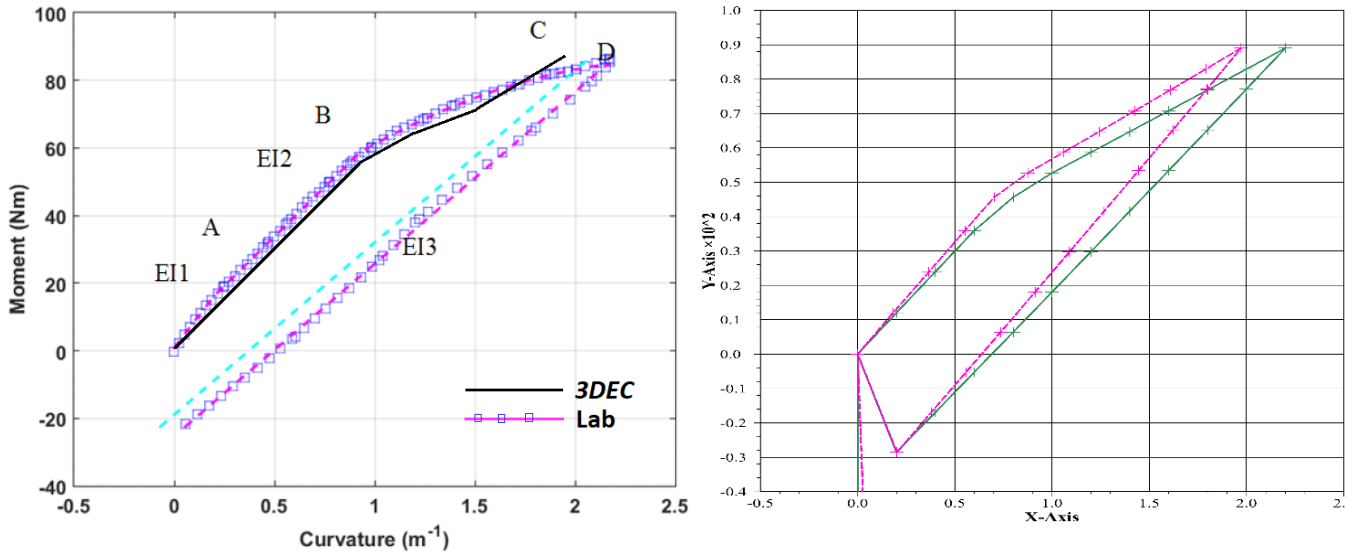

Figure 2-5 Moment-curvature response of a single fuel rod obtained from laboratory tests (left) and from *PFC* model (right).

2.2.3 Degradation of Nozzles, Canister/Overpack, and Spacer Grids

The order of degradation of the basket internals is based on the corrosion lifetime information discussed in Section 2.1, and has six degradation stages:

1) Aluminum-based basket plates would fail first.
2) Stainless steel nozzle blocks would then fail, whereupon they would not constrain transverse movement of the fuel rods, or any movement of the guide tube ends.
3) The stainless steel canister shell and internal basket supports would then fail, but the circular fuel/basket envelope geometry would be maintained by the overpack and the backfill external to the waste package.
4) After many thousands of years, spacer grids would begin to fail under load. This stage could have a duration of many thousands of years.
5) After tens to hundreds of thousands of years the fuel rods would begin to break as the cladding thickness is reduced by corrosion, and bending occurs from spacer grid failure.
6) Eventually, the guide tubes would break as the wall thickness is reduced by corrosion, and bending occurs from loading by slumping fuel.

Note that the degradation times are order-of-magnitude approximations used only to set the sequence in which different components degrade in the model.

The aluminum-based basket plates will fail first. The thin-walled canister shell and the internal basket supports (between the shell and the basket) will fail next, before the overpacks and the spacer grids fail.

The fuel rod cladding and spacer grids are made of similar material with similar thickness. However, the spacer grids support the weight of the fuel assemblies and will fail under load before degrading completely. The structure of actual spacer grids is very detailed, including thin plates, dimples, and springs to hold the fuel rod, as shown in Figure 2-6. Representation of complete details would be computationally prohibitive. Instead, the spacer grid is currently modeled as a rectilinear array of plates (Figure 2-4). The thickness of plates modeled is larger than the actual thickness such that the boundary condition that the rods have no free room available to move in the plane normal to their axis is simulated correctly. However, the density of the plates is reduced accordingly to match the mass of the spacer grid.

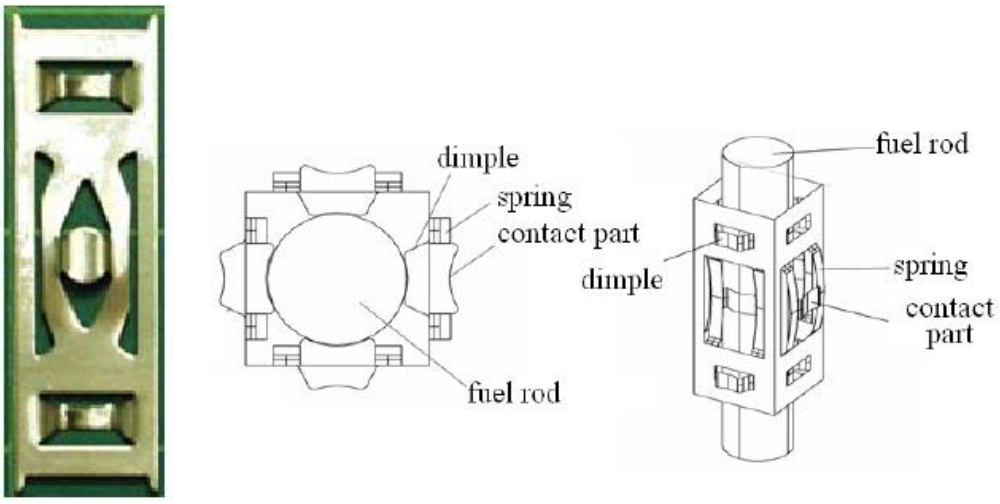

Figure 2-6 Details of a single cell of spacer grid (Lee et al. 2007).

Modeling the degradation of spacer grids by discretizing them along the thickness of the plate is also not feasible due to the computational cost involved. A different approach will therefore be used whereby the intact spacer grid that is under the greatest load (without looking at the detail of stress concentrations) fails, and more grids are failed successively using the same criterion to examine the mode of degradation. This will be done once the basket plates and end nozzle connections have failed, but with constraint from the canister and overpack, and prior to failure of fuel rods or guide tubes. It is proposed to allow failure in shear and hinge formation only at the joints making up the spacer grid (Figure 2-2). The approach is an approximation of potentially complex modes of spacer grid failure, which can be revisited in a future study once the successive-failure approach is better understood.

Simulations have been carried out using the 2.5-D model where the basket plates are degraded first, followed by spacer grids under the highest load for each degradation stage listed above. As a first approximation, the degradation is modeled by completely weakening all the internal bonds, causing failure at all the joints of that component (i.e., either a basket plate or spacer grid). None of the components are deleted from the model, but are maintained in their failed condition to preserve the total mass in the model. The results are shown in Figures 2-7 through 2-9. Simulations of this type with the detailed 2.5-D model require roughly a day to run on an updated Windows workstation, with failure of the basket plates and all spacer grids. Calculating responses to seismic ground motion takes far longer with the detailed model, but can be done using the simplified model (SNL-ICG 2019). The numerical formulation is fully explicit finite difference, with time step optimization (Itasca 2016; 2018).

Discretization of spacer grids (SGs) in the vertical direction was very coarse for these simulations and can be improved in future work. Where any spacer grids are carrying the same load, they are failed in the same step, particularly in early steps (e.g., step SG-1 in Figure 2-7). Some grid failures are less noticeable where the fuel is supported by the canister shell or basket supports. Note that at degradation steps SG-3 and SG-4, weakening the spacer grids in the middle does not lead to any

significant change in the overall configuration. Only after weakening the spacer grids on the sides in SG-5 and the grid above in SG-6 are significant changes in configuration seen.

Corresponding movement of the PWR assembly guide tubes as the spacer grids are successively weakened and the stack collapses, is shown in cross-section for the same 2.5-D degradation steps SG-1 through SG-16, in Figures 2-10 through 2-12. Simulated degraded configurations with individual fuel rods and guide tubes containing disposal control rods could be used to evaluate the reactivity of modified PWR assemblies after basket plate degradation and spacer grid failures.

A measure of degraded configuration for reactivity analysis that is suggested here is the spatial density of guide tubes (which may contain disposal control rods). This is represented in Figure 2-13 using a color-coded scheme. The number of guide tubes in each cell of a fixed 7-cm regular grid is indicated by color, for degradation steps SG-11 through SG-16 (corresponding to Figures 2-9 and 2-12).

The successive weakening and collapse of spacer grids in a basket with failed basket plates under gravity is a first approximation to the evolution of the canister internal configuration. Other modes of degradation are possible, for example ground motion of sufficient magnitude could cause rearrangement or breakage of fuel rods, and rearrangement or falling of fuel assemblies into large voids formed. Note that the preliminary results of Figures 2-7 through 2-9 are from the 2.5-D model, and that other modes of deformation, failure, rearrangement and voiding may be found with the full 3-D model.

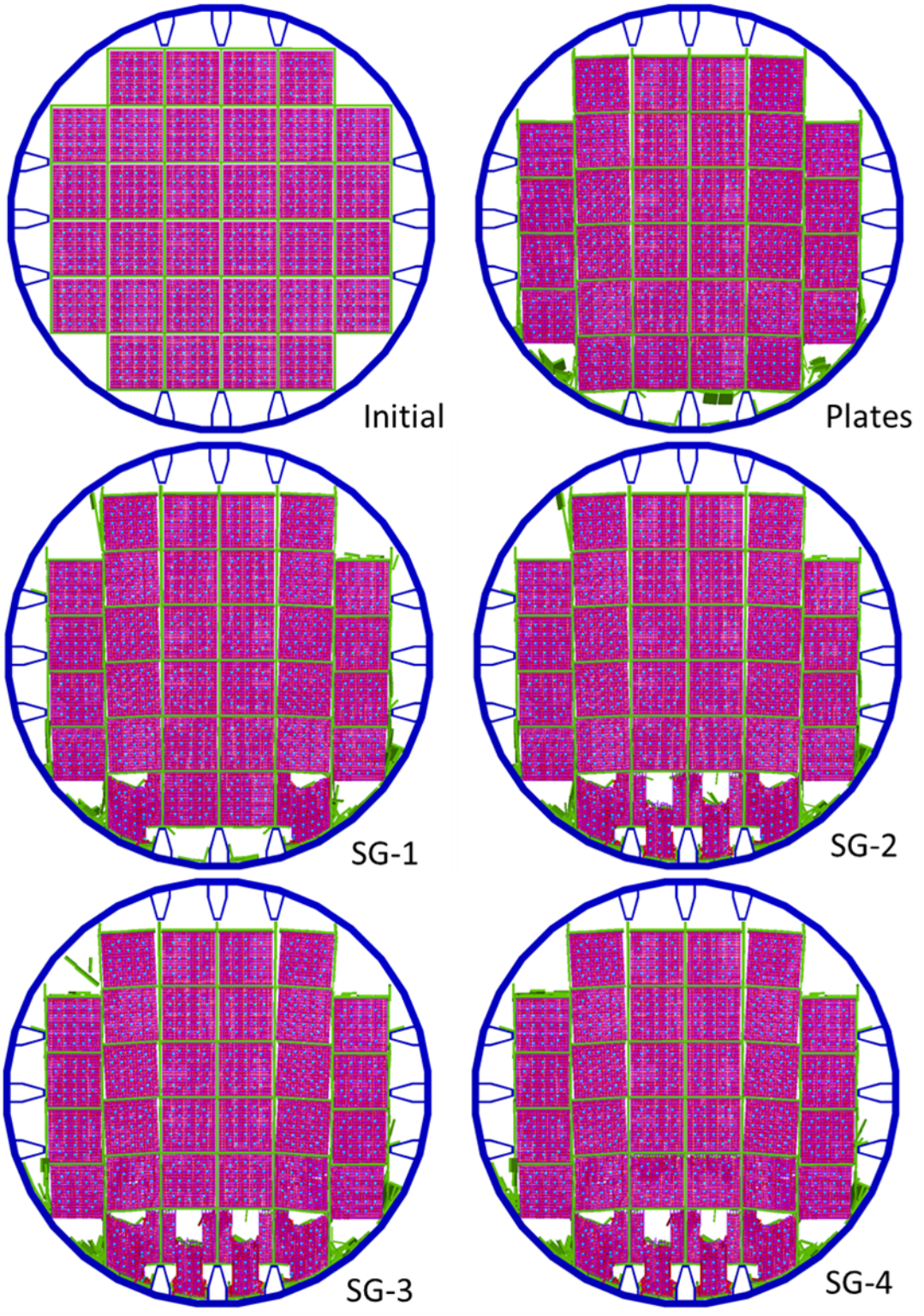

Figure 2-7 Internal configuration of the canister (2.5-D model) initially, with basket plates degraded, and with successive degradation of 4 spacer grids (SG-1 through SG-4).

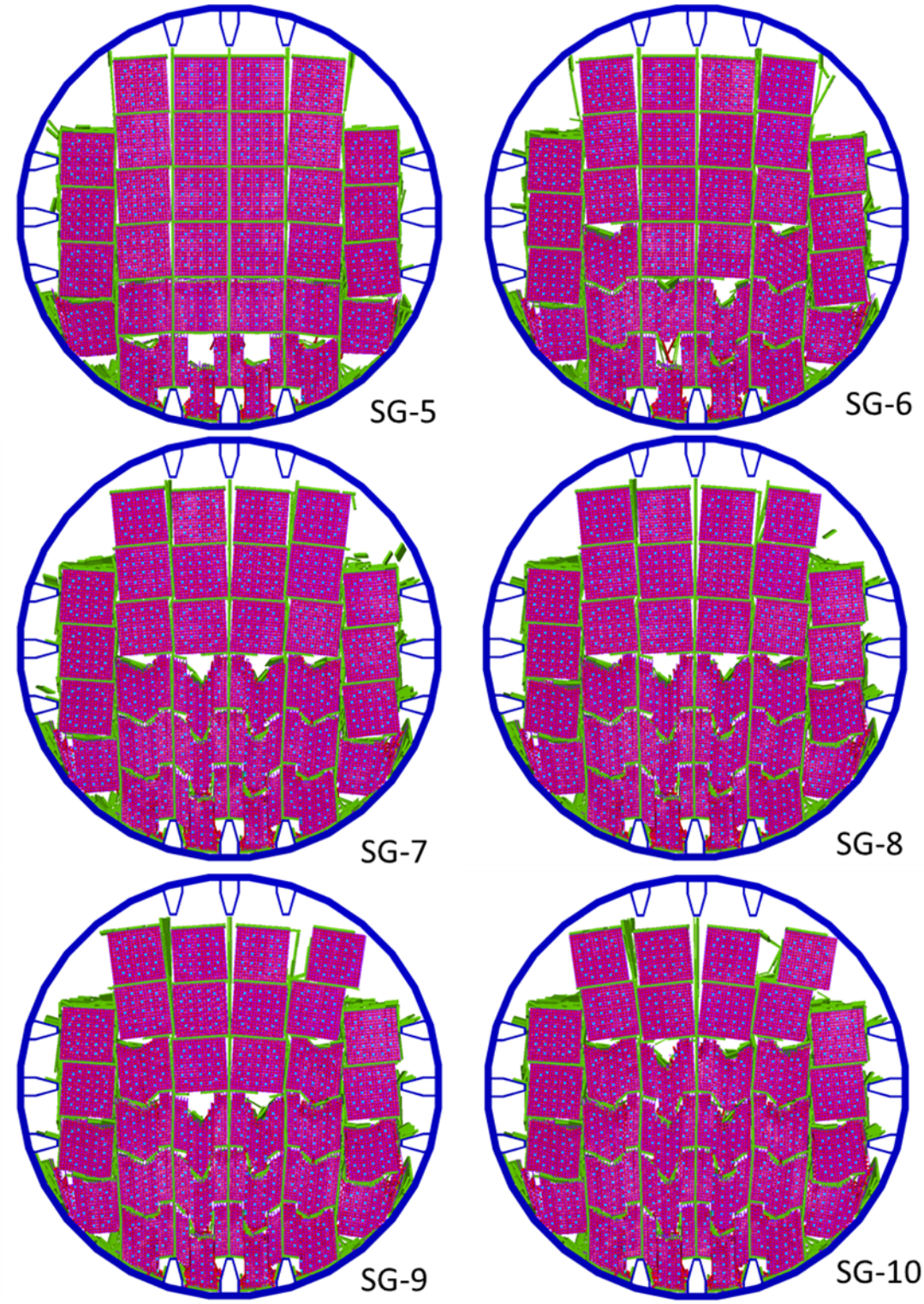

Figure 2-8 Internal configuration of the canister (2.5-D model) with successive degradation of 6 more spacer grids (SG-5 through SG-10).

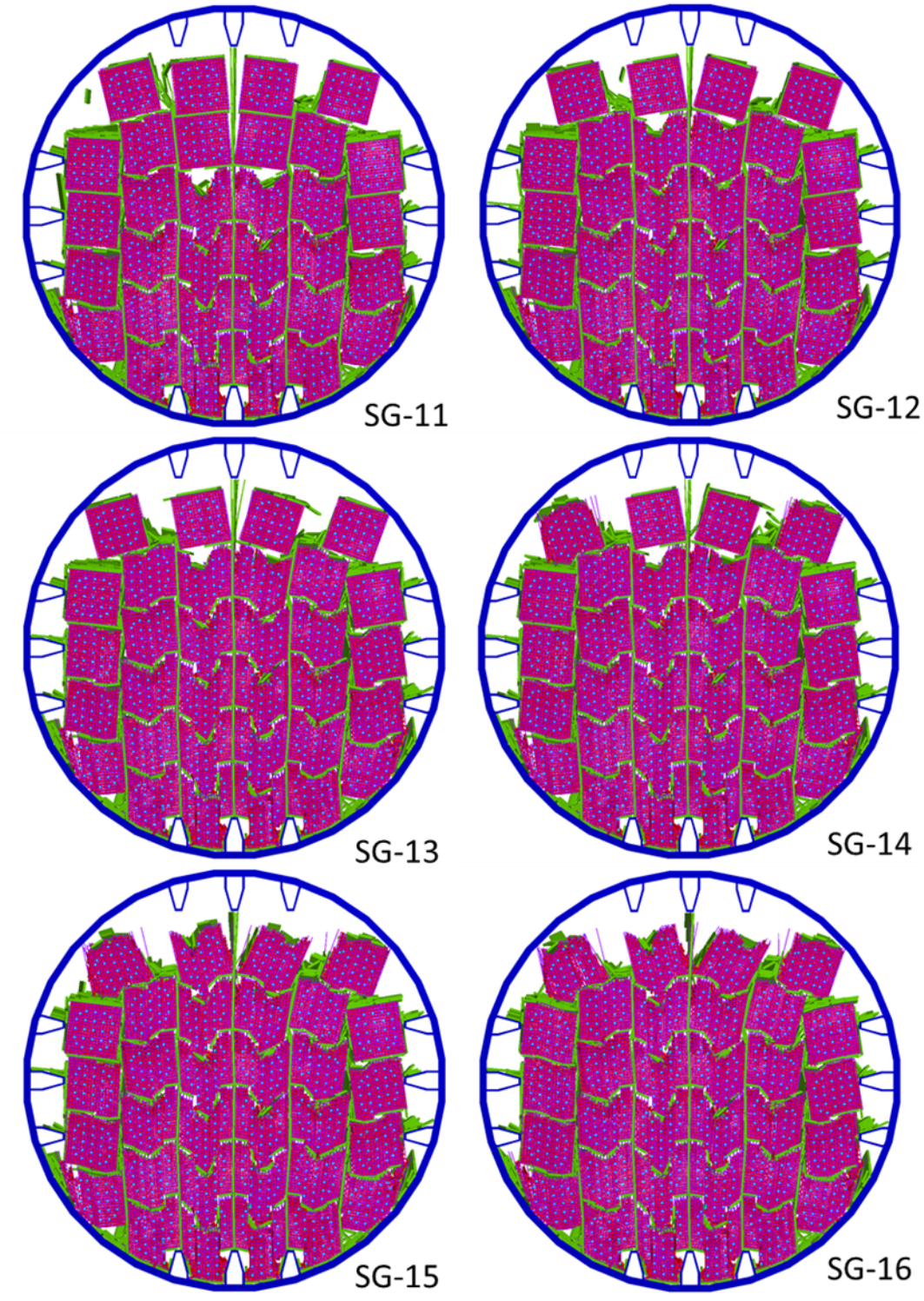

Figure 2-9 Internal configuration of the canister (2.5-D model) with successive degradation of 6 more spacer grids (SG-11 through SG-16)

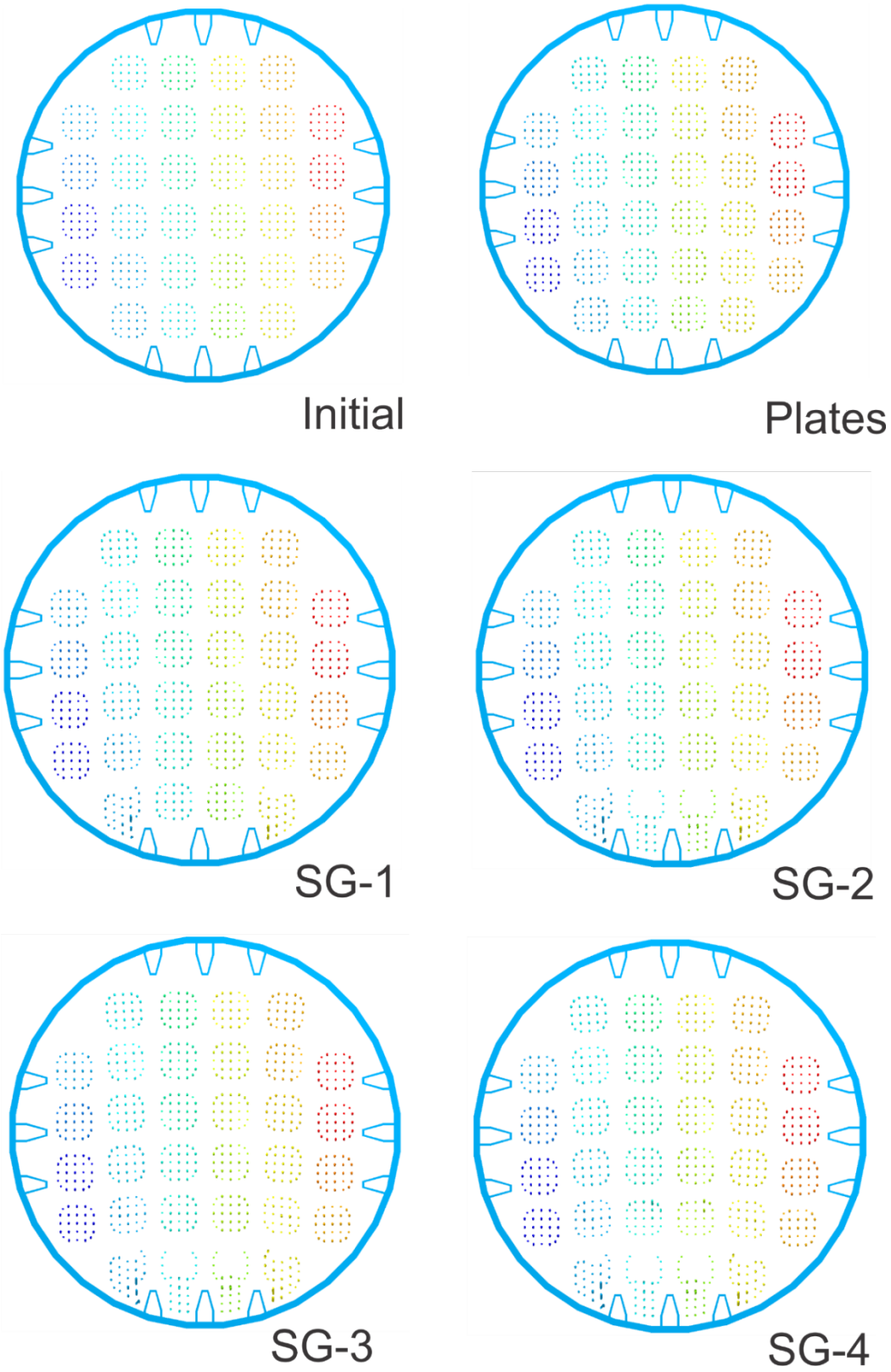

Figure 2-10 Positions of PWR assembly guide tubes in cross-section, initially, with basket plates degraded, and with successive degradation of 4 spacer grids (SG-1 through SG-4).

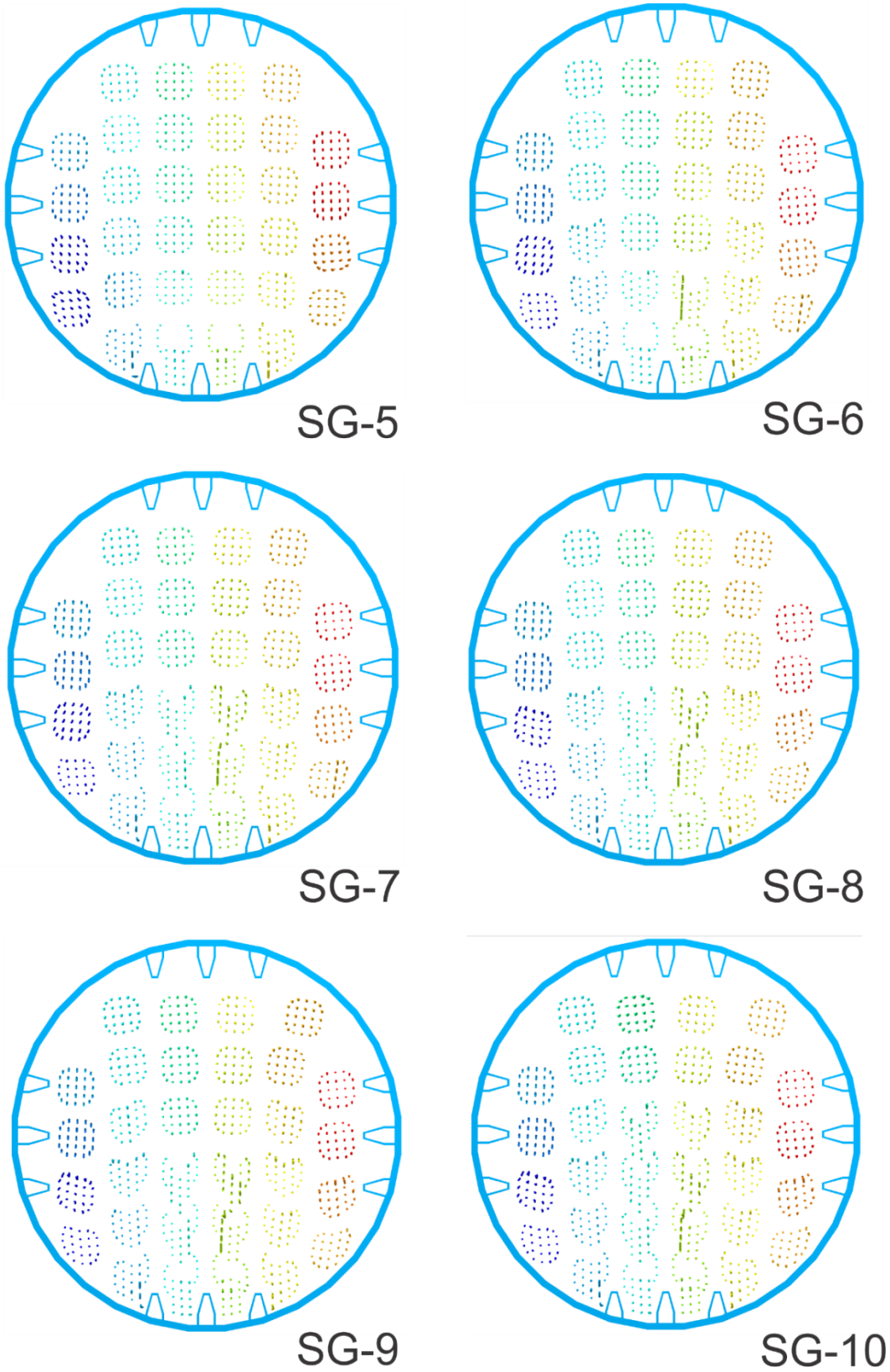

Figure 2-11 Positions of PWR assembly guide tubes in cross-section, with successive degradation of 6 more spacer grids (SG-5 through SG-10).

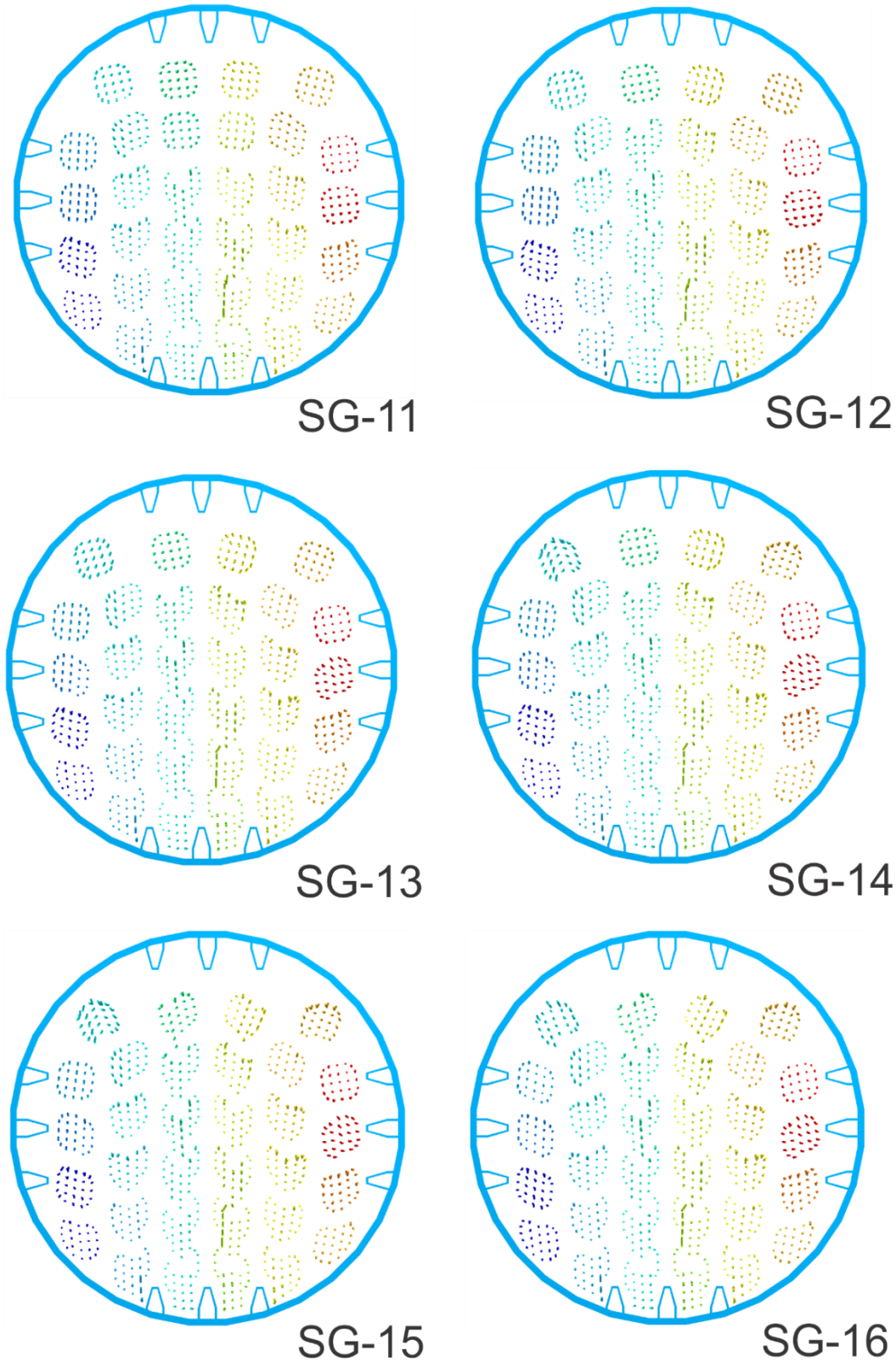

Figure 2-12 Positions of PWR assembly guide tubes in cross-section, with successive degradation of 6 more spacer grids (SG-11 through SG-16).

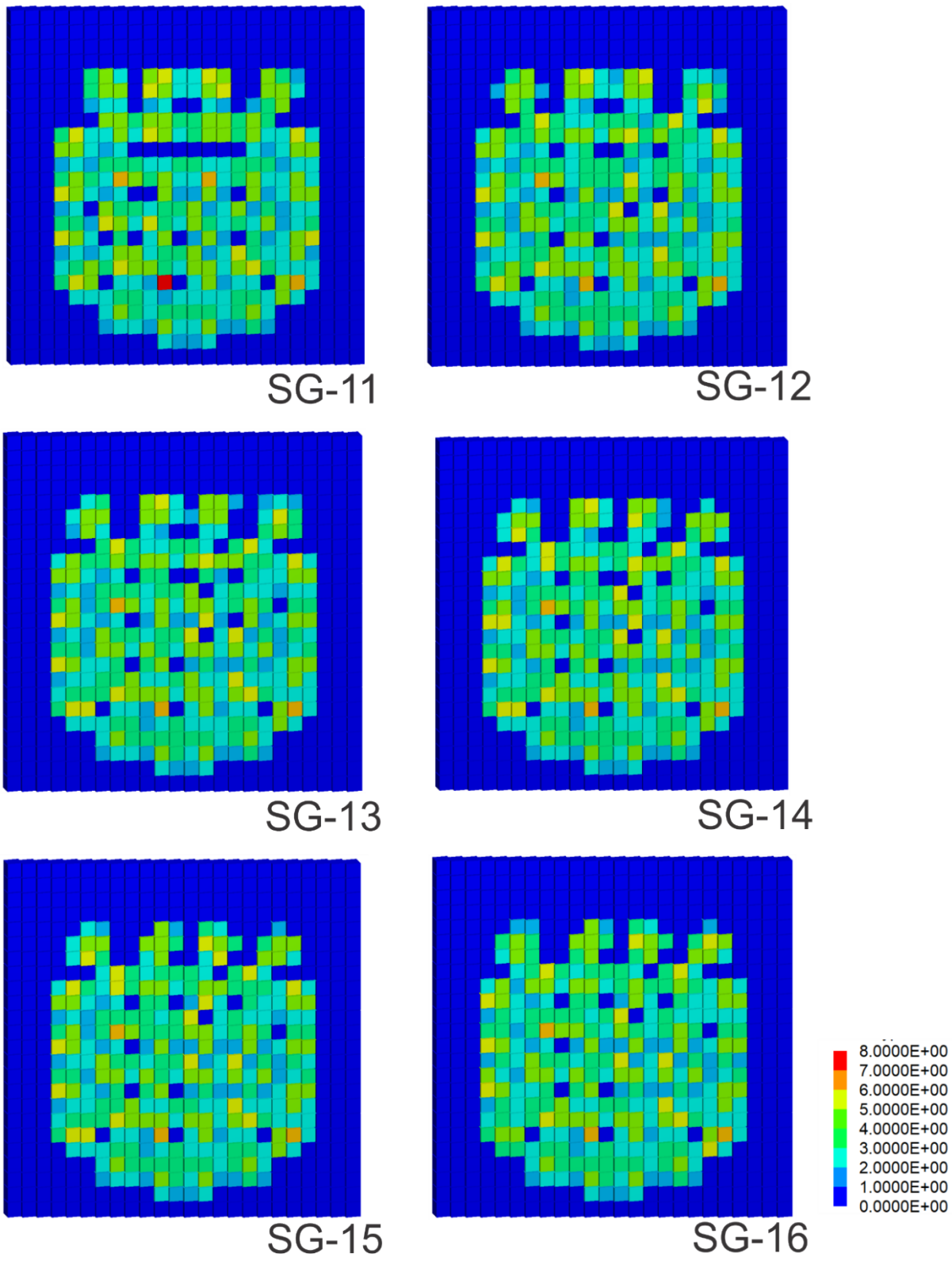

Figure 2-13 Color-coded plot of the numbers of PWR guide tubes (disposal control rods) in each cell of a regular grid, for degraded configurations SG-11 through SG-16.

3. Progress Report on Waste Package Breach Model

3.1 Modeling Plan

This document describes the work plan for Task 2 of the Itasca Numerical Study of Nuclear Waste Canister Degradation. The task is described in the work plan as:

> The purpose of the Waste Package Breach Model is to study the formation of cracks in the stainless steel DPC shell, and their properties particularly in response to internal pressurization of the canister. Previous work on this model represented pressurization as a quasi-steady step-function increase. Crack deformation and growth were estimated, and the venting rate for water flow from the breach under pressure was estimated. For this scope of work the following features shall be added to the Waste Package Breach Model:
>
> - Represent the interior of a DPC as a finite saturated reservoir constrained by the canister shell, and subject to pressure increase when heat is added;
> - Perform sensitivity studies to determine at what event energy and duration, and crack behavior, does pressure decay so that boiling can occur in a saturated waste package; and
> - Couple canister shell and overpack crack behavior, and (separate) mechanical and flow behavior of a compliant medium external to the waste package.

The remainder of this planning section expands on this description and gives more details of planned work tasks.

To date, the Waste Package Breach Model has two components: 1) a model to investigate the quasi-static mechanical response of a fractured canister or overpack to internal pressurization; and 2) a zero-dimensional thermal-hydraulics model to predict pressure, deformation, and water outflow from a canister or overpack during a criticality event. These are referred to as Models 2A and 2B in the following discussion.

Model 2A: Quasi-Static Response of a Fractured Container to Internal Pressurization – The initial work looked at a canister and overpack with a pre-existing hoop or longitudinal fracture of a given length. A limitation of this analysis was the lack of a backfill material, so that the canister could deform into free space with no resistance.

- Task 2A-1: This model will be extended to consider a compliant medium surrounding the canister. The surroundings will be represented either as *FLAC3D* zones or as local springs attached to each grid-point. In either case, material properties will be selected to be representative of typical back fill materials. Both bentonite and crushed rock back fill will be considered.
- Task 2A-2: Generate quasi-static mechanical response curves for a representative set of pre-fractured canisters and overpack scenarios. The response should give volume, fracture aperture, and fracture length as a function of pressure.

Model 2B: Zero-Dimensional Thermal-Hydraulic Model – A lumped capacitance model for canister heating and pressurization was developed. The model considers a single temperature for the water and canister internals. Planned tasks include:

- Task 2B-1: Implement two-phase behavior. The current model is only for liquid water. When boiling starts, vapor bubbles and liquid co-exist and the pressure volume relation is constrained to the saturation curve. The vapor and liquid water will be assumed to be well mixed.
- Task 2B-2: Investigate super-critical water states to make sure the model works. Beyond the critical point in water, there is no distinction between the liquid and vapor phase. Some modification to the water equation of state (EoS) may be needed to handle transitions into this region.
- Task 2B-3: Extend the model to consider heat transfer, mass transfer, and pore pressure dissipation in the surrounding backfill. As a first approximation consider the surrounding as a one-dimensional spherically symmetric domain.
- Task 2B-4: Run a sensitivity study of different sized criticality events. Criticality events ranging in size from 10^{12} to 4×10^{19} fissions (32.4 J to 1.23 GJ) over times of 1, 10, 100 seconds will be considered.
- Task 2B-5: Run a high-energy transient case consisting of power ramped from zero to 50 GW over 10 msec, then back to zero in 10 msec (total 10^3 GJ).

3.2 Summary of Modeling Progress

This section summarizes progress on modeling of the effects from internal heating of a DPC by a criticality event, on deformation of the canister shell and overpack, and the internal temperature and pressure. The same generic 32-PWR DPC described previously was assumed (mainly the dimensions of the shell). As described in Section 2.2, eventually the overpack and shell will be breached by initial fractures, which could allow ground water to fill the canister. If the canister internals, including neutron absorber components, are sufficiently degraded by exposure to ground water, a criticality event could occur. Such an event would create transient elevated internal temperature and pressure conditions. The short-term power of a transient criticality event could be orders of magnitude greater than quasi-steady events (comparing estimates for the power of steady events with transient criticality accidents; Price et al. 2019 and McLaughlin et al. 2000). Rapid energy releases inside a flooded DPC could cause the canister shell and overpack to deform, and the initial fractures to grow, affecting hydraulic transmissivity with the surroundings. It is important to understand the change in transmissivity for two reasons. First, it could have significant influence over the nature of criticality events, including their energy and repeat frequency, and secondly, because it will control the release of radionuclides from the canister. For criticality events in a geologic repository negative feedback from Doppler broadening and negative changes in water density is expected to be limited, so that criticality events will be limited mainly by boiling (Davidson et al. 2019, Appendix A.2). Constraining fluid escape during a transient event could suppress boiling and increase the event power and duration so that the system reaches much higher temperature, and releases much greater total energy.

This section describes progress on the waste package breach model since the last report (SNL-ICG 2019). Progress includes accounting for backfill in the mechanical response of the DPC to internal pressurization and in the venting of fluid from the DPC, coupled with a zero-dimensional thermal-hydraulic model to predict the pressure history and mass flow out of the DPC. Figure 3-1 shows an overview of the waste package breach model, and subsequent sections describe each aspect of

the model. The schematic of the canister model used for the simulation of deformation and fracture propagation and the model results (contours of displacement magnitudes) are shown in Figure 3-2.

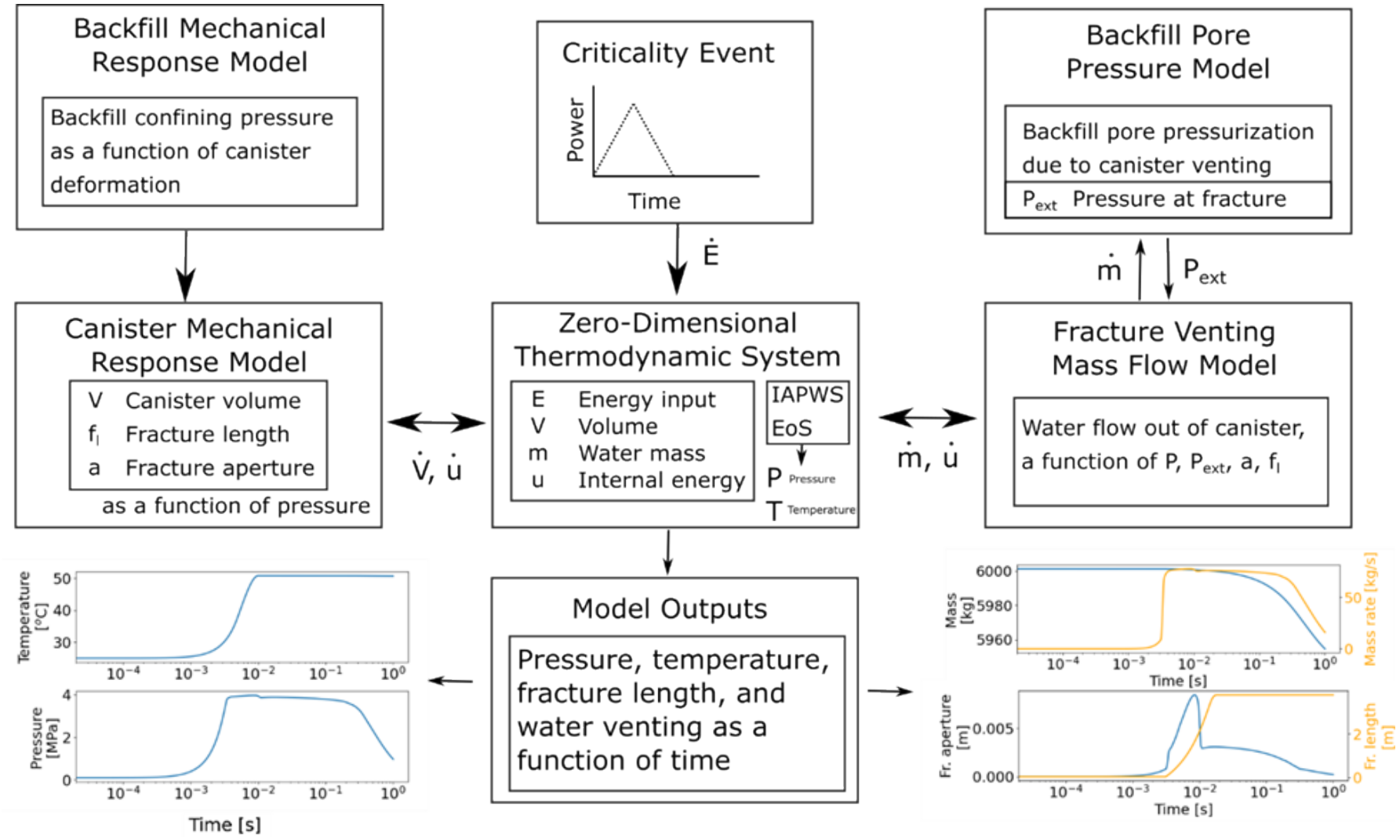

Figure 3-1 Overview of waste package breach model components.

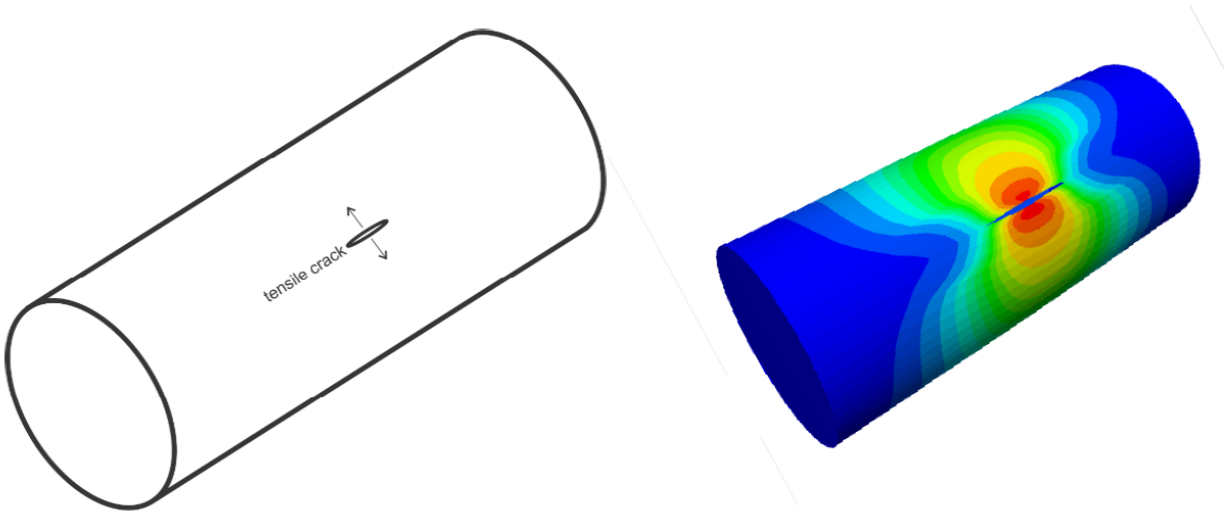

Figure 3-2 Schematic of waste package breach model along with results (contours of displacement magnitudes).

3.2 Previously Reported Waste Package Breach Model

Previous model development is summarized in Section 1.2.3. In short, the container (DPC shell or overpack) was represented by a hollow cylinder with ends, using the *FLAC3D* simulation code (Itasca 2019). The model was parameterized to simulate deformation, yielding, and fracturing of the shell or overpack. An initial fracture was assumed, and pressure acting on the inner surface of the canister was increased incrementally, solving for quasi-static mechanical equilibrium at each pressure increment. The applied pressure is the differential of internal minus external pressures. The model was run for a canister (1.2 cm thick) and an overpack (2.45 cm thick).

Results showed that the package can fail by extension of the fracture (along a predetermined path in the model setup) or by plastic yielding. Depending on the initial fracture orientation, location, and length, the package fails by fracture growth or by yielding, whichever process starts at a lower internal pressure. Regardless of the failure mechanism, the package has a critical failure pressure (less than 15 MPa) beyond which the package is unable to contain increases in pressure. In the previous work only the mechanical response of the canister or overpack was considered and the effects of backfill were not considered.

3.3 Representing Backfill in the Mechanical Model

The disposal concepts for direct disposal of commercial spent nuclear fuel (SNF) in DPCs include some type of backfill surrounding the waste package. Support provided by the backfill will reduce the canister deformation as the canister is internally pressurized. Representing the canister, backfill, and disposal drift directly as *FLAC3D* zones would significantly increase the computational effort. To avoid that, the backfill is represented as a set of springs connected to the outer *FLAC3D* grid points that resist outward normal deformation of the canister. The spring constant is determined via numerical experiment using a *FLAC3D* model of backfill material. The model is a cylindrical annulus with an inner radius of 0.88 m and an outer radius of 2.64 m. Two symmetry planes with roller boundary conditions are used to reduce the model size. The backfill is represented as a linear elastic material with Young's modulus values of 100 MPa and 300 MPa,

Poisson ratio of 0.1, and density of 1,400 kg/m^3. These values are appropriate for both bentonite and crushed rock backfill. A single grid point on the inner radius is loaded with a constant outward radial force. The model is solved, and the grid point radial displacement is measured. This is conceptually similar to a Winkler foundation analysis (Bowles 1997). The procedure is repeated for an increasing series of outward forces. As expected, the results show a linear relation between applied force and displacement. Interpreting this as a pressure (by considering the effective surface area of the grid point) gives a constant of 0.38 GPa/m for a Young's modulus of 100 MPa and 1.14 GPa/m for a Young's modulus of 300 MPa. Figure 3-3 shows the backfill mechanical model and the pressure as a function of displacement.

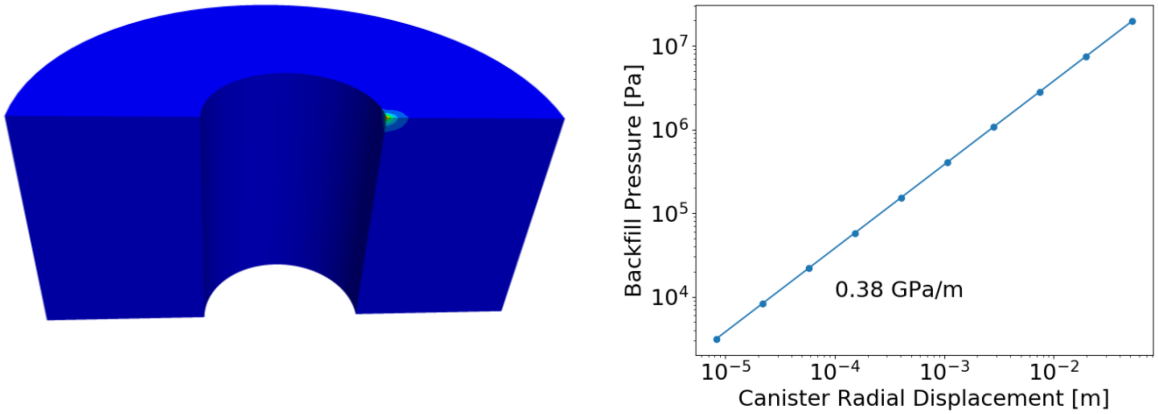

Figure 3-3 Backfill mechanical model and liner mechanical response for a backfill with a Young's modulus of 100 MPa.

3.3.1 Mechanical Response Functions

The next step is to predict the canister pressure history and the mass flow out of the canister during a heat-generation (criticality) event. It would be computationally expensive and complex to couple a thermal-hydraulics model to the *FLAC3D* waste package breach model, so a decoupled approach is taken. As the *FLAC3D* model of the vessel (canister or overpack) is pressurized, mechanical response curves describing the vessel volume, average fracture aperture, and fracture length are recorded. These mechanical response curves are shown in Figure 3-4. Two distinct regions separated by the critical failure pressure are observed. Before the critical failure pressure, the mechanical response is linear and relatively stiff. There is a nonlinear failure region where the fracture is growing followed by another linear but relatively soft region.

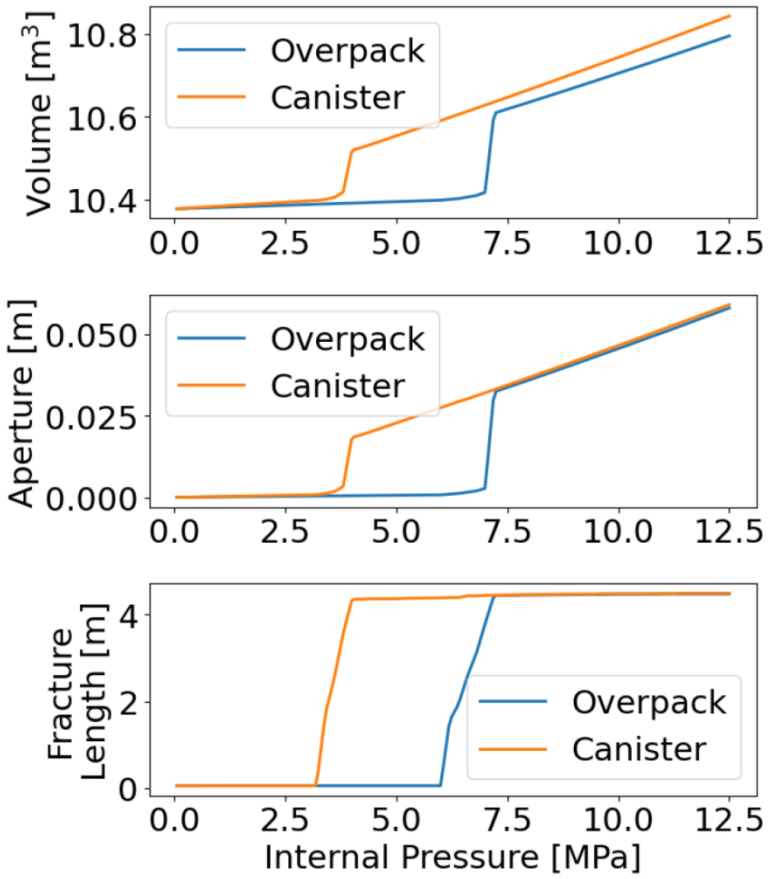

Figure 3-4 Mechanical response curves for a canister and overpack with a centered longitudinal fracture with 5 cm initial length.

3.3.2 Mechanical Effects of the Backfill

To understand the effect of backfill on the mechanical response of the waste package, it is instructive to look at the mechanical response curves described in the previous section with and without the backfill present. Figure 3-5 shows the mechanical response curves for a canister with and without backfill. The backfill has several effects: 1) it makes the canister stiffer; 2) it delays the onset of fracturing; and 3) it prevents large deformations at high pressures beyond the critical failure pressure (i.e., after fracture propagates for the entire length of the DPC).

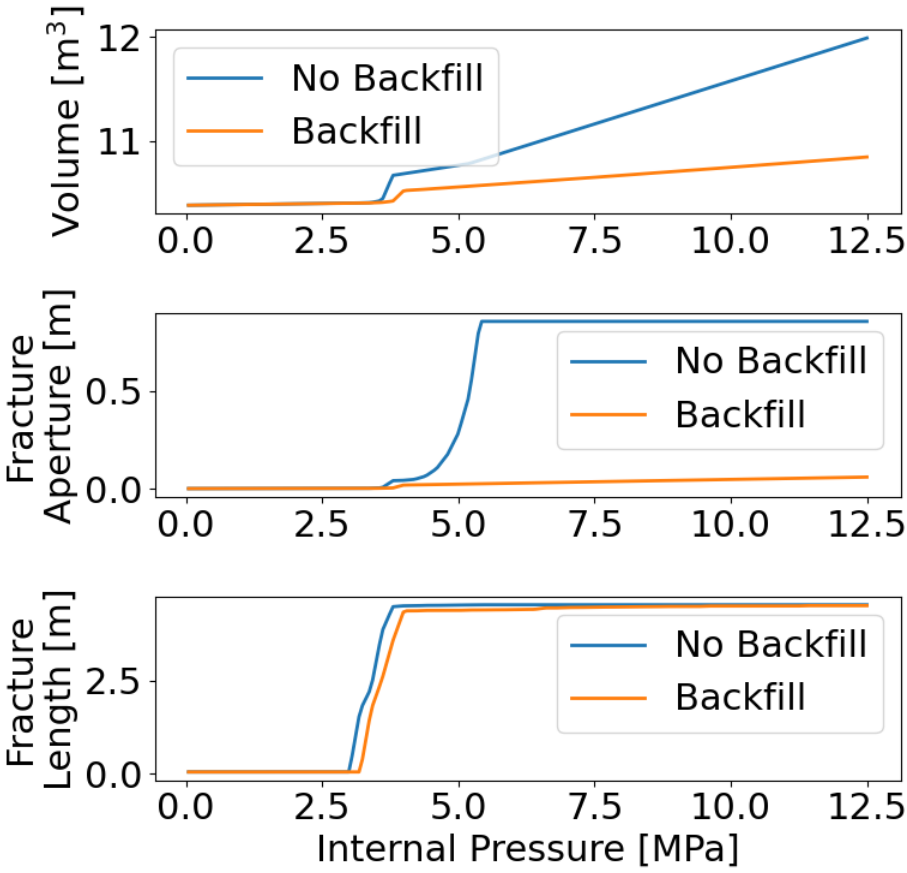

Figure 3-5 Mechanical response curves with and without backfill surrounding a canister.

3.4 Zero-Dimensional Thermal-Hydraulic Model

A simplified thermal-hydraulic model has been developed to predict the vessel pressure, vessel deformation, and mass flow out of the vessel as a function of time during and after a criticality event. The model is kept as simple as possible to allow a fast run time. The model presented in this section does not represent spatial gradients of pressure or temperature. A zero-dimensional lumped approximation is taken where a single temperature and pressure describe the water inside the vessel. The metals inside the vessel are treated as incompressible. As energy from a criticality event enters the system, the metals and water are heated, but only the water changes volume. The water in the vessel is treated as a thermodynamic system, which can undergo three changes: 1) heating from a criticality event; 2) adiabatic expansion of the vessel; and 3) flow of water out of the system into the backfill. There is a characteristic time proportional to the vessel radius divided by the water P-wave speed above which the assumption of uniform equilibrium pressure is reasonable. For the canister and overpack considered in this study, the characteristic time is around half a millisecond. The model unknowns are given in Table 3-1. Derived quantities and model inputs are given in Table 3-2.

Table 3-1 Unknowns of the Zero-Dimensional Model

Symbol	Quantity	Units
U	Specific internal energy of the water in the vessel	J/kg
V	Vessel (canister or overpack) volume	m^3
m_f	Mass of water in vessel	kg
E_C	Total energy input from criticality event (model input)	J

Table 3-2 Derived Quantities and Model Inputs

Symbol	Quantity	Units
$p_c(t)$	Criticality power as a function of time (model input)	J/sec
l_f	Fracture length	m
a	Fracture aperture	m
P	Water pressure	Pa
T	Water temperature	°C
ρ_w	Water density	kg/m^3
u	Water venting velocity	m/sec

3.4.1 Heating Due to Criticality

The rate of change of the total energy added due to criticality is

$$\dot{E}_C = p_C(t)$$

where $p_c(t)$ is a prescribed function giving the criticality power as a function of time. The thermodynamic state of the water in the canister is described by a density and a specific internal energy. From these two properties, pressure, temperature, and other thermodynamic variables can be calculated from the IAPWS EoS (IAPWS 2018). In the model, the water density is taken as the mass of water in the vessel divided by the vessel volume ($\rho_w = m_f V$). The model is currently only for liquid water, although work is underway to extend the model to two-phase conditions.

The change in the water-specific internal energy is

$$\dot{u} = \frac{1}{m_f}\left(\dot{E}_C f_h - \left(\dot{V}P + \frac{1}{2}\dot{m}_f u^2\right)\right)$$

The term $\dot{E}_C f_h$ represents energy input from the criticality event, the term $\dot{V}P$ represents mechanical work done by the water to expand the vessel and the term $\frac{1}{2}\dot{m}_f u^2$ represents the mechanical work to accelerate water out the fracture. f_h is the fraction of the criticality energy that goes toward heating the water. Assuming the criticality energy is evenly and instantly partitioned between the metals in the vessel and the water this fraction is

$$f_h = \frac{f_w \rho_w C_{pw}}{f_w \rho_w C_{pw} + (1 - f_w)\rho_m C_{pm}}$$

where f_w is the mass fraction of water in the canister at the initial state. This quantity is only calculated once before the model is run. The model parameters are listed in Table 3-3. The lumped

values for the metal are taken as weighted averages of the uranium dioxide, zirconium, aluminum, and steel inside the vessel.

Table 3-3 Model Parameters

Symbol	Quantity	Value
f_w	Mass fraction of water in vessel	0.58
ρ_w	Density of water	997 kg/m^3
C_{pw}	Specific heat capacity of water	4181.3 J/kg/°C
ρ_m	Lumped density of vessel internal metal	8244 J/kg/°C
C_{pm}	Lumped specific heat capacity of vessel internal metal	385 J/kg/°C

3.4.2 Representing the Canister Mechanical Response

Three functions are introduced to represent the mechanical response of the vessel to internal pressurization. The functions $M_v(P)$, $M_{fl}(P)$ and $M_a(P)$ are piecewise linear interpolants of the canister volume, fracture length, and mean fracture aperture as a function of internal pressure. These functions are fit to the mechanical response curves shown in Figure 3-4. The metal inside the vessel is treated as incompressible, so all vessel volume change is taken up by the water. For numerical convenience, a fictitious dimensionless timescale for vessel deformation is introduced:

$$\dot{V} = Ae^{B\left|M_v(P)-V\right|} - 1$$

where the constants A and B are selected so the volume change is fast relative to all other processes in the model. In all the cases, A = 3.7×10^{-2} and B = 150. Fracture aperture change is treated as instantaneous in the model. Mode I fracture growth is rate-limited by the material Rayleigh wave speed. In steel, the Rayleigh wave speed is around 1,000 m/sec. An approximate timescale for fracture growth rate (m/sec) is introduced:

$$\dot{f}_l = \begin{cases} 1{,}000\left(1 - e^{-5(M_{fl}(P)-f_l)}\right) & M_{fl}(P) > f_l \\ 0 & else \end{cases}$$

No heat transfer by conduction with the surroundings is considered. This is an acceptable approximation for the short times the model is run for.

3.4.3 Mass Flow into the Backfill

As the water pressure rises, water is forced out of the vessel into the backfill. This mass transfer is treated as turbulent fracture flow across the thickness of the vessel. The pressure drop due to flow along a fracture with flow length L, corresponding to wall thickness, is

$$\frac{P - P_{ext}}{L} = \frac{f\rho_w v_w u^2}{2D_h}$$

$$f = \left(0.79log_{10}(Re) - 1.64\right)^{-2}$$

$$Re = u/(D_h v_w)$$

$$D_h = 2M_a(P)$$

where P_{ext} is the pressure outside the vessel (described in the next section), L is the vessel wall thickness, ρ_w is the density of water, v_w is the water kinematic viscosity, u is the water velocity, f

is the drag coefficient, and D_h is the hydraulic diameter. The drag coefficient is an empirically derived function of Reynolds number (Re). For a given fracture aperture and pressure drop between the interior and exterior of the vessel, the water velocity, u, is found by a numerical root finding algorithm. This velocity is representative of true conditions when u is less than the local sound speed in water. At higher driving pressures, compressible effects become important and, neglecting any geometric effects, the velocity asymptotically approaches the sound speed. To account for this effect, the velocity of the water flowing out of the fracture is limited to less than 300 m/sec. This limit is typically not reached because the backfill pressurization, described in the next section, limits the mass flow before velocities approach the sound speed. The rate of change of the mass of water in the vessel is

$$\dot{m} = \rho_w u M_a(P) M_{fl}(P)$$

where ρ_w is the density of water and M_a(P) and M_{fl}(P) are the fracture aperture and length functions described above.

3.4.4 Backfill Pressure

As high internal pressures push water out of the vessel, the backfill surrounding the vessel will pressurize, limiting the pressure difference between the vessel and the backfill. Although crushed rock has relatively high hydraulic diffusivity (relative to other media around the waste package) the timescales of the criticality events are short and the backfill will pressurize. Similar to the approach taken to represent mechanical response of the backfill, a separate three-dimensional model is created to represent fluid flow and pore-pressure dissipation in the backfill. Figure 3-6 shows the model geometry and an example pore-pressure solution. The vessel is implicitly represented as an empty cylinder in the middle of the model. The pore pressure on the top surface of the model is fixed, and water flows into the backfill along the fracture in the vessel. The model is time-dependent and allows the fracture to grow, causing fluid to be injected over a larger area. The backfill flow model presented in this section does not consider any mechanical deformations, and the backfill mechanical response model described in Section 3 does not consider any pore pressurization effects. The backfill is assumed to be fully saturated and the storativity is taken as the elastic storage only. The hydraulic properties of the backfill are listed in Table 3-4.

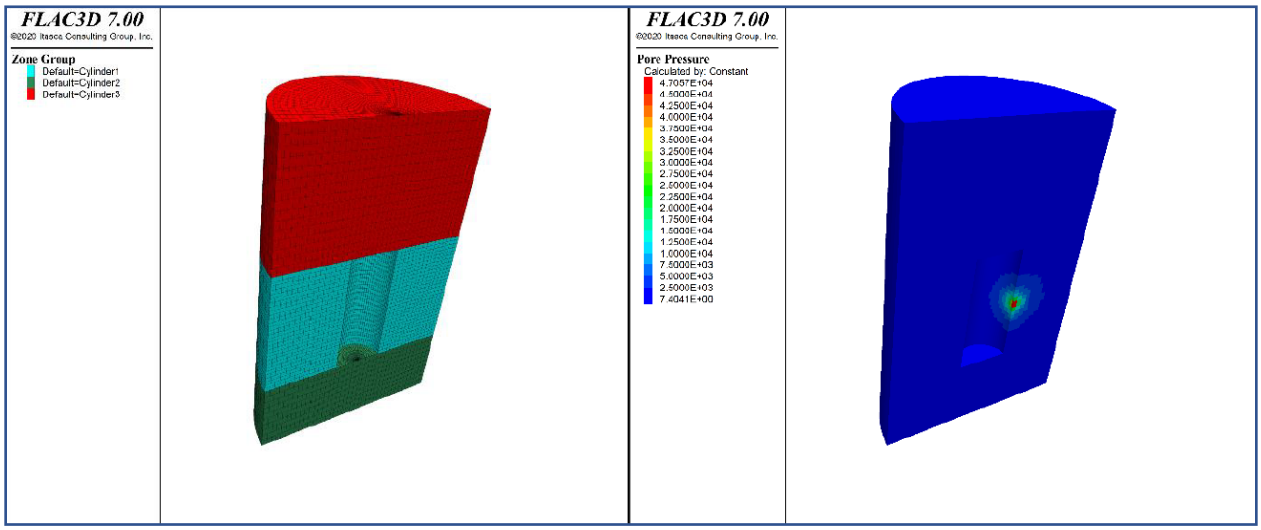

Figure 3-6 Model geometry and sample solution for backfill flow model.

Table 3-4 Hydraulic Properties of the Backfill

Symbol	Quantity	Value	Source
k_H	Hydraulic conductivity	$5 \times 10^{-4}\ m/sec$	Assumed
K	Mobility coefficient	$\frac{k_H}{\rho_w g} = 5.11 \times 10^{-9} \frac{m^2}{Pa - sec}$	Calculated
E	Backfill Young's modulus	100 MPa	Assumed
v	Poisson ratio	0.1	Assumed
M	P-wave modulus	$M = \frac{E(1-v)}{(1+v)(1-2v)} = 102.3\ MPa$	Calculated
S	Storativity	$\frac{1}{M} = 9.8 \times 10^{-9} Pa^{-1}$	Calculated
c	Pore pressure diffusivity	$c = \frac{k}{S} = 5.2 \frac{m^2}{sec}$	Calculated
t_c	Characteristic time for pore pressure dissipation over 1 meter	$t_c = \frac{(1\ m)^2}{c} = 0.2c$	Calculated

Symbol	Quantity	Value	Source
k_H	Hydraulic conductivity	$5 \times 10^{-4}\ m/sec$	Assumed
K	Mobility coefficient	$\frac{k_H}{\rho_w g} = 5.11 \times 10^{-9} \frac{m^2}{Pa - sec}$	Calculated
E	Backfill Young's modulus	100 MPa	Assumed
v	Poisson ratio	0.1	Assumed
M	P-wave modulus	$M = \frac{E(1-v)}{(1+v)(1-2v)} = 102.3\ MPa$	Calculated
S	Storativity	$\frac{1}{M} = 9.8 \times 10^{-9} Pa^{-1}$	Calculated
c	Pore pressure diffusivity	$c = \frac{k}{S} = 5.2 \frac{m^2}{sec}$	Calculated
t_c	Characteristic time for pore pressure dissipation over 1 meter	$t_c = \frac{(1\ m)^2}{c} = 0.2c$	Calculated

Sample solutions for fixed injection rates are shown in the left plot of Figure 3-7. The pressure in the backfill (at the fracture) increases rapidly and approaches a steady state after around 1 second of injection. By the time a steady state is reached, the pressure increase due to injection has reached the upper boundary in the model. Different model geometries or boundary conditions will give different time histories of backfill pore pressure. Higher injection rates give higher steady state

injection pressures. The right plot in Figure 3-7 shows the steady state injection pressure as a function of injection rate.

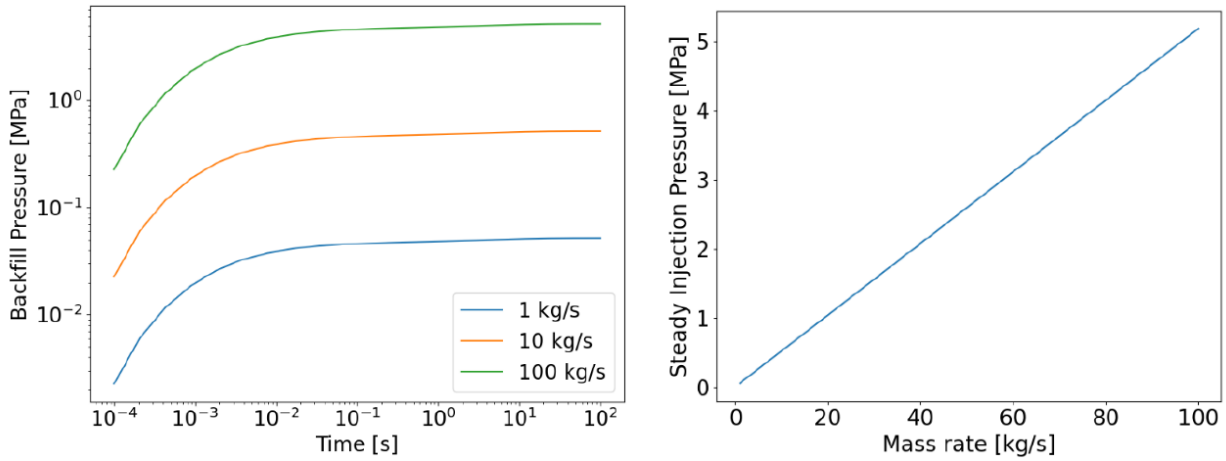

Figure 3-7 Sample solutions of backfill pore pressure.

The backfill flow model is coupled with the zero-dimensional thermal-hydraulic model. As a first approximation to representing the backfill pore pressure in the zero-dimensional model, the flow in the backfill is assumed to always be steady state. The right plot in Figure 3-7 is used to determine the external pressure for a given mass flow rate. This plot is used to determine the value of P_{ext} used in the mass flow calculation described in Section 3.4.3. For times shorter than the characteristic pore pressure dissipation time of 0.2 sec, this approach will overestimate the backfill pore pressure (and underestimate the mass flow). Future work involves a more direct coupling between these effects that will give a more accurate mass flow (and more reliable estimates of pressure and temperature).

3.4.5 Model Solutions

The equations described above are a set of coupled ordinary differential equations that are easily solved numerically. Figure 3-8 shows four canister-model solutions in pressure-volume space to demonstrate the solution regimes that are possible. These are solutions for the case of venting of the canister that is not backfilled. In the top left plot, pressure initially increases linearly with temperature, then more slowly starting around 2 MPa. The criticality event stops when pressure reaches 2.6 MPa and finally drops back down to the starting pressure. The top right plot is similar, but the system enters a near constant pressure heating regime at 3.2 MPa before dropping at the end of the criticality event. Similarly, the bottom right plot enters a near constant pressure heating regime until the saturation line is intersected (and boiling starts) around 240℃. The bottom right plot shows the effect of cyclical criticality events, with the end of the final event causing boiling by decompression. Heating from the criticality event causes thermal expansion in the water, and the volume change is taken up by mechanical deformation of the canister and by water venting out of the canister (mass flow). The initial deviation of pressure from a linear trend is caused by mass flow increasing. The near constant pressure heating regime is entered when the canister begins to fail. After failure, the canister is less stiff, and the fracture is longer and has a larger aperture. Each of these effects limits the pressure inside the canister. It is difficult for the canister to support

internal pressures beyond the critical failure pressure as additional internal load is accommodated by (softer) canister expansion and (faster) mass flow. The trend for the overpack is the same but the failure critical pressure is higher.

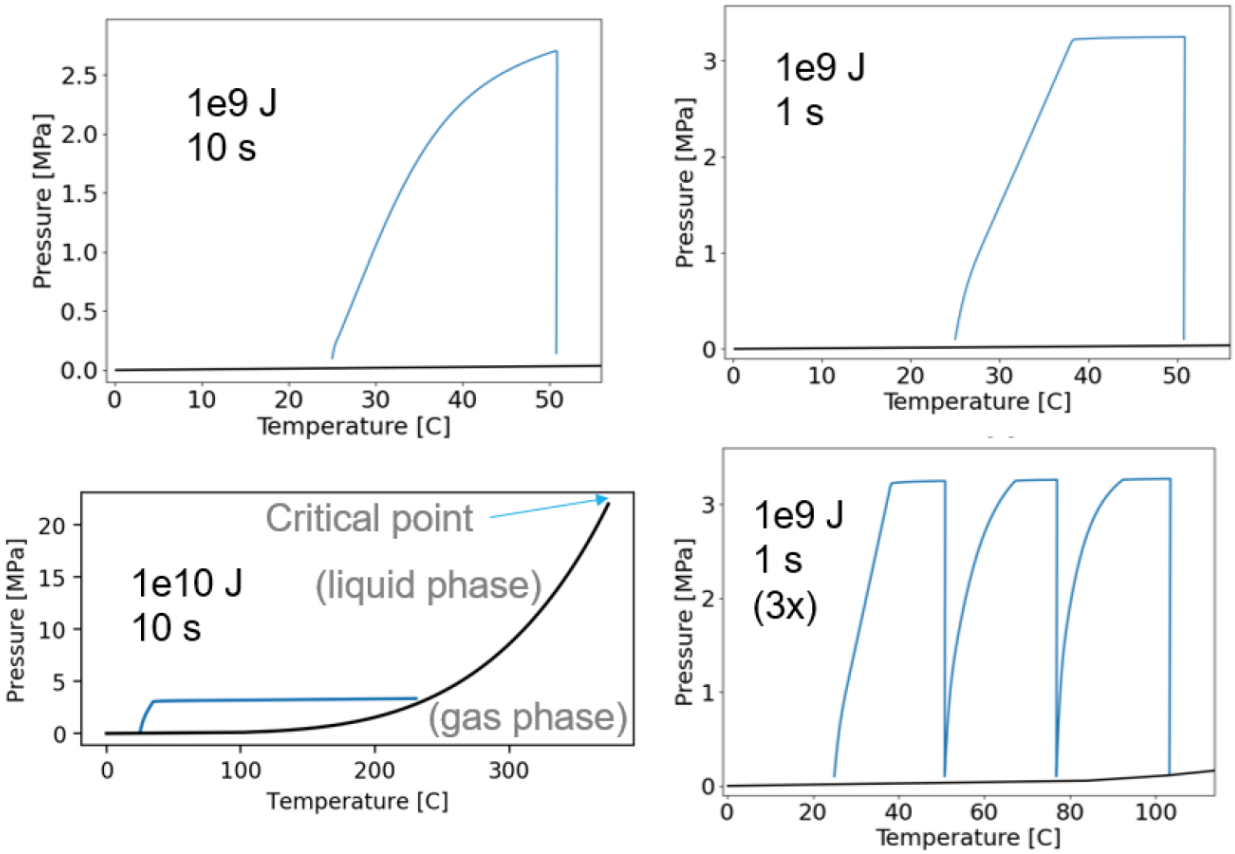

Figure 3-8 Four model solutions in pressure-volume space.

3.4.6 Detailed Solution for a Realistic Criticality Event

A criticality event 10 msec in duration that releases 1 GJ of energy is considered in this section. The event power function, $p_c(t)$, is an equilateral triangle function with a base width of 10 msec, a peak at 5 msec, and a total energy of 1 GJ. The effect of vented fluid dissipation through the backfill is accounted for in this example. Figures 3-9 and 3-10 show the results as a function of time for the canister and overpack cases, respectively. Both cases follow similar trends, but the overpack case reaches a higher pressure because the overpack can withstand higher pressures before the onset of mechanical failure. Although the mass flow rate is higher in the overpack case, the total mass of water flowing out of the system is the same. Note that the temperature increase in the two cases is the same. A parametric study was done to determine the threshold in event energy that will cause fracture growth. For the assumption that the event energy is release over 10 msec, with peak power at 5 msec, and the power function being an equilateral triangle, events with total energy less than 0.2 GJ do not cause fracture growth (for the 5-cm longitudinal fracture in the center of a canister). This event energy limit will depend on several factors including the

initial fracture size, the fracture orientation and location, cannister versus overpack, and the rate that the energy is released.

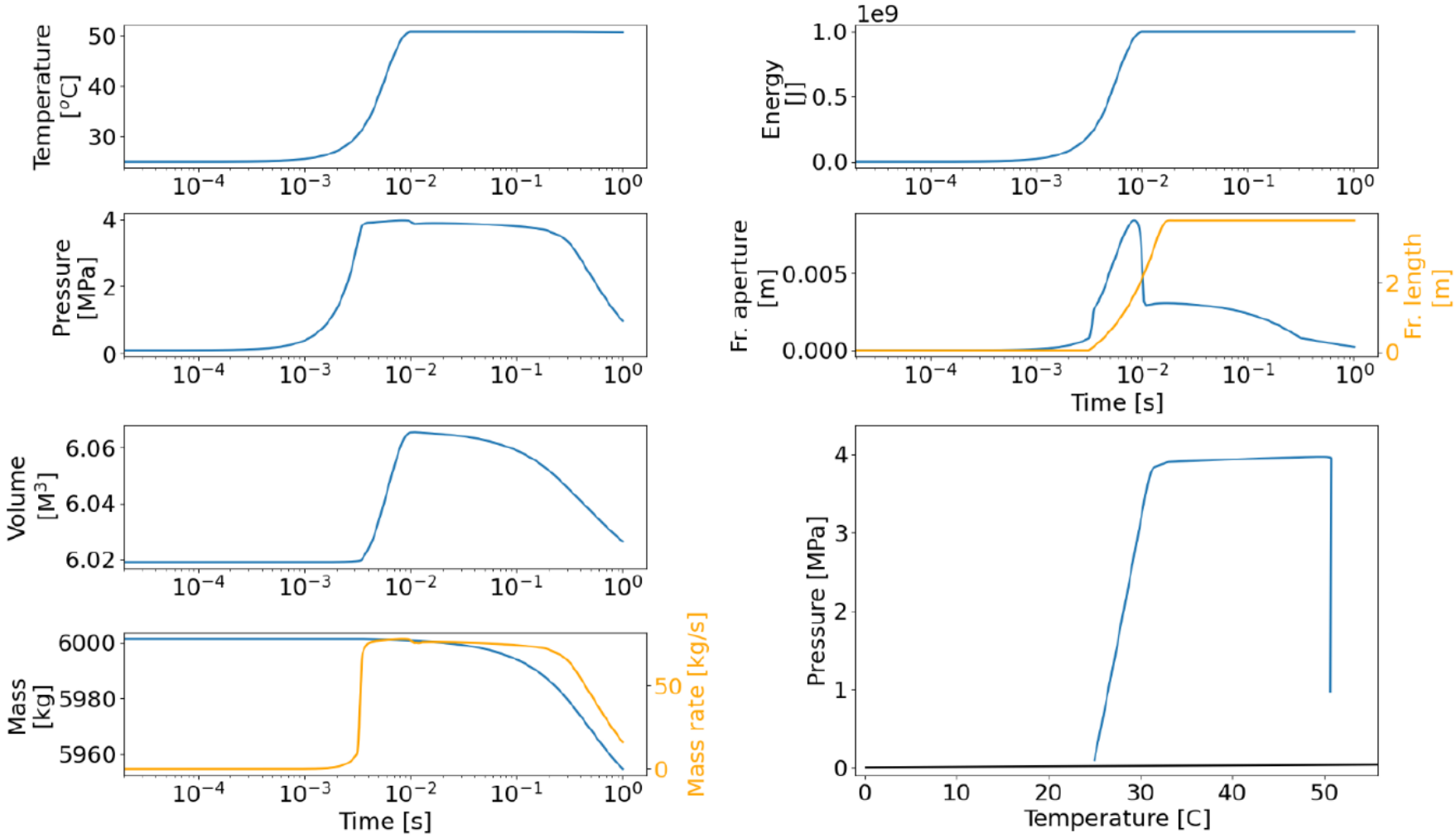

Figure 3-9 Detailed model solution for a canister subjected to a 1 GJ criticality event over 10 msec.

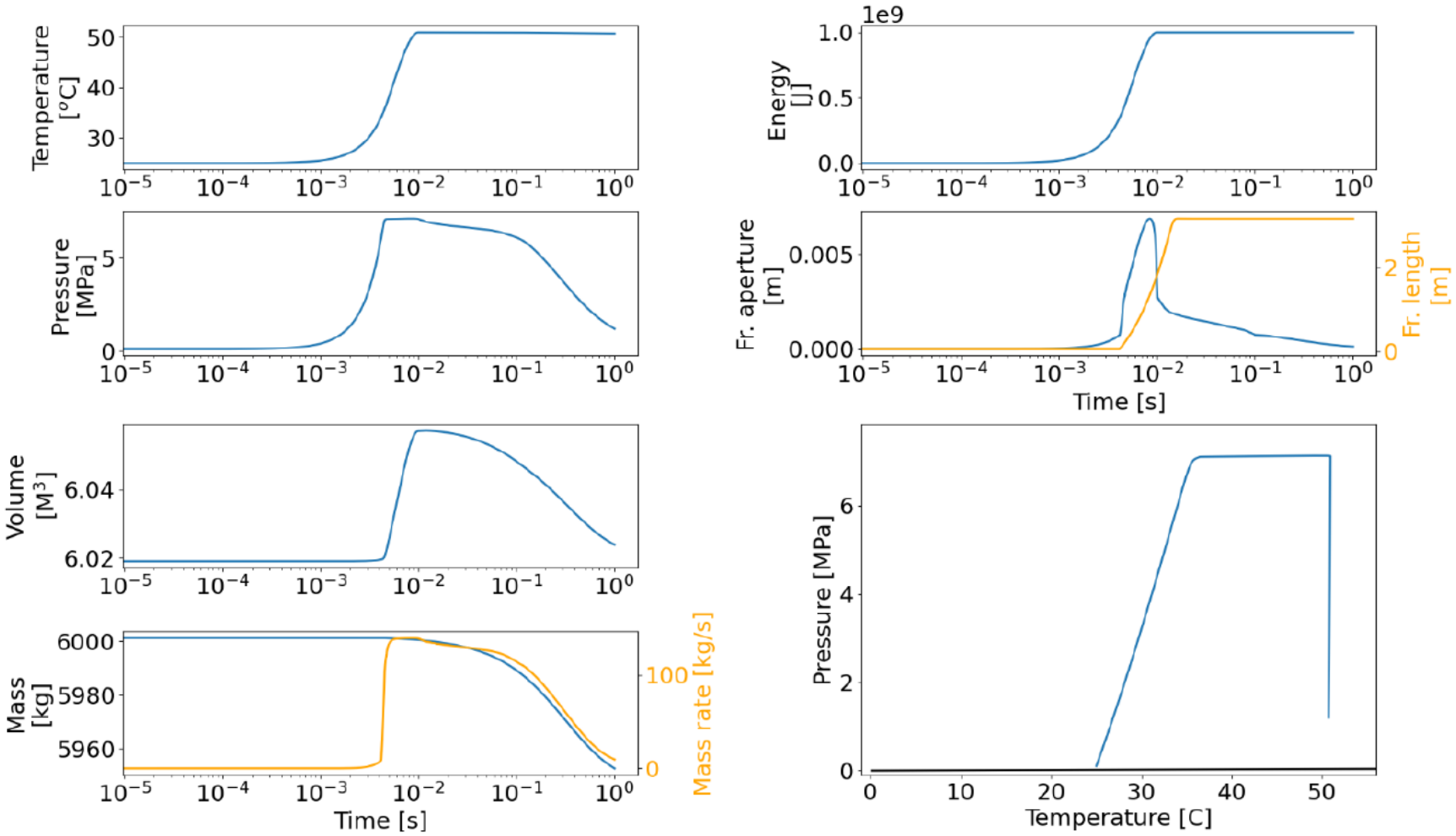

Figure 3-10 Detailed model solution for a thicker overpack subjected to a 1 GJ criticality event over 10 msec.

4. Progress Report on DPC Crush Model

4.1 Modeling Plan

A new model is being developed to study the potential for collapse of the DPC shell and basket in response to external hydrostatic loading (prior to breach and flooding of the DPC). Aspects to be included are:

- Initial conditions of intact fuel/basket and canister shell, internal pressure (gas) of 1 to 5 bars.
- Yield/rupture constitutive models for SS304 shell and aluminum basket plates.
- Include canister shell and internals (basket and fuel), externally loaded, with constraint of the DPC shell by a thicker, breached overpack.
- Estimate external pressure required for collapse of the DPC shell, and possibly basket and fuel, and the mode of failure.

The approach is based on an assumption that the overpack is designed so that collapse of the overpack (and the DPC) is not plausible under expected repository conditions, including loading from ground water pressure, buffer/backfill swelling and rock (opening and closure) deformation.

The geometry of the basket model is constructed assuming a generic 32-PWR egg-crate style basket with aluminum-based plates, similar to that depicted in Figure 4-1. The rationale for this selection is that: 1) degradation in ground water will proceed fastest with the aluminum-based basket; 2) PWR fuel is more reactive than BWR fuel; and 3) the 32-PWR size is common. The width and height of each cell are assumed to be 0.21 m, which is approximate based on the inner diameter of the canister, the number of cells, and the geometry.

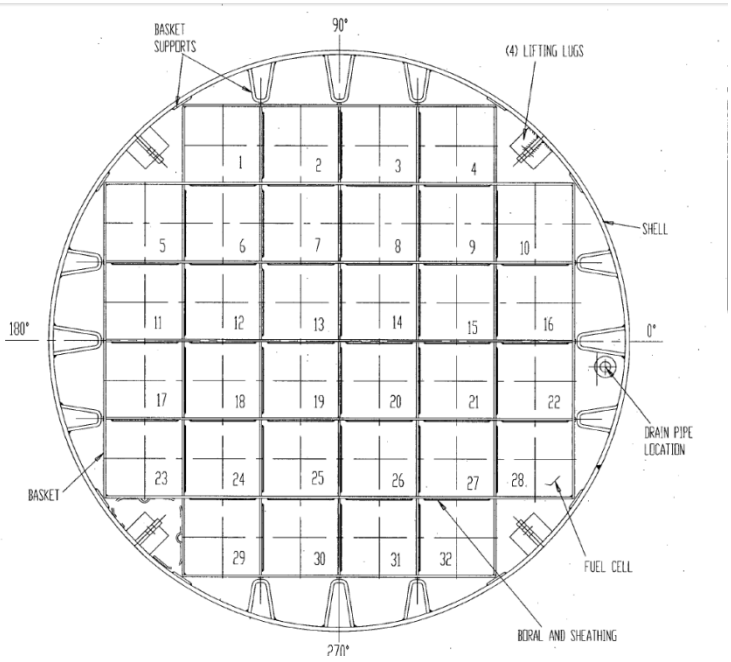

Figure 4-1 Cross-section view: Geometry of the basket (from Figure 1.2.4 of Holtec 2018).

The geometries of the fuel assembly and rods are shown in Figures 4-2 and 4-3. A 17×17 PWR assembly with 25 guide tubes is considered. The diameter of the fuel rods and inner and outer dimeters of the cladding are specified in Figure 4-3. The fuel type is assumed to be uranium oxide, and the cladding is assumed to be Zircaloy.

The *FLAC3D* model (Itasca 2019) assumes symmetries along the canister axis, representing a section from the middle of the spacer grid to the half-distance of two spacer grids (Figure 4-4). Consequently, the model will not account for the effect of the lids on the stiffness and strength of the DPC. It is reasonable to assume that the effect of the lids in a section in the middle of the DPC will be relatively small. The DPC is located inside the cylindrical overpack, which in this analysis is assumed to be rigid. The maximum gap between the DPC and the overpack is assumed to be 2 cm. The external load is applied as the hydrostatic pressure on the outside surface of the canister shell.

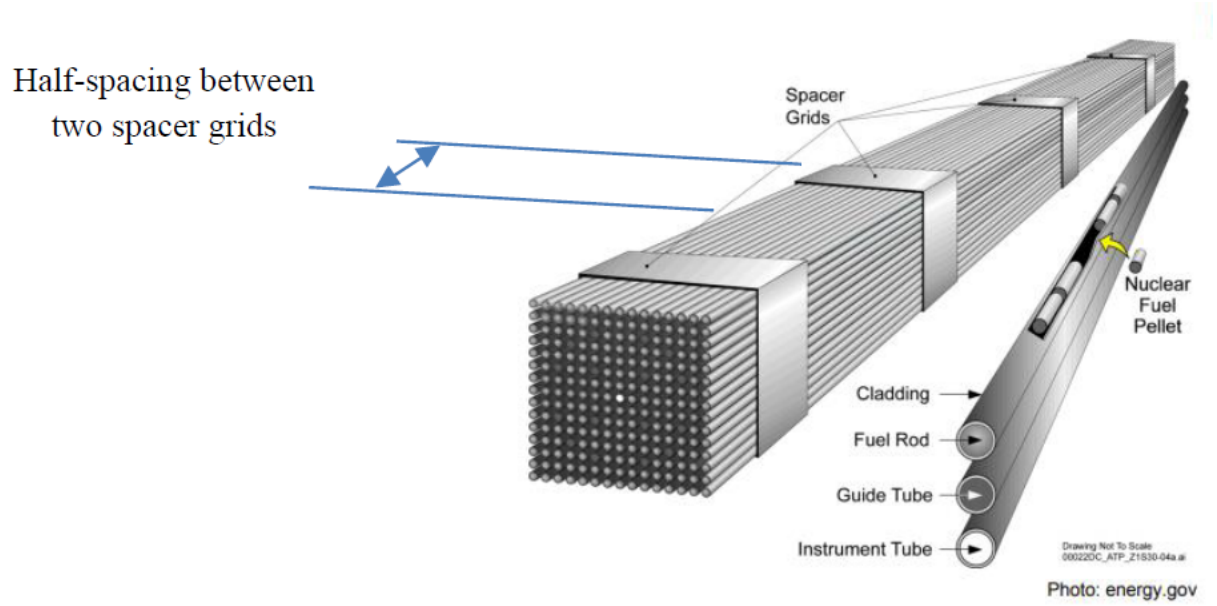

Figure 4-2 Geometry of the fuel assembly.

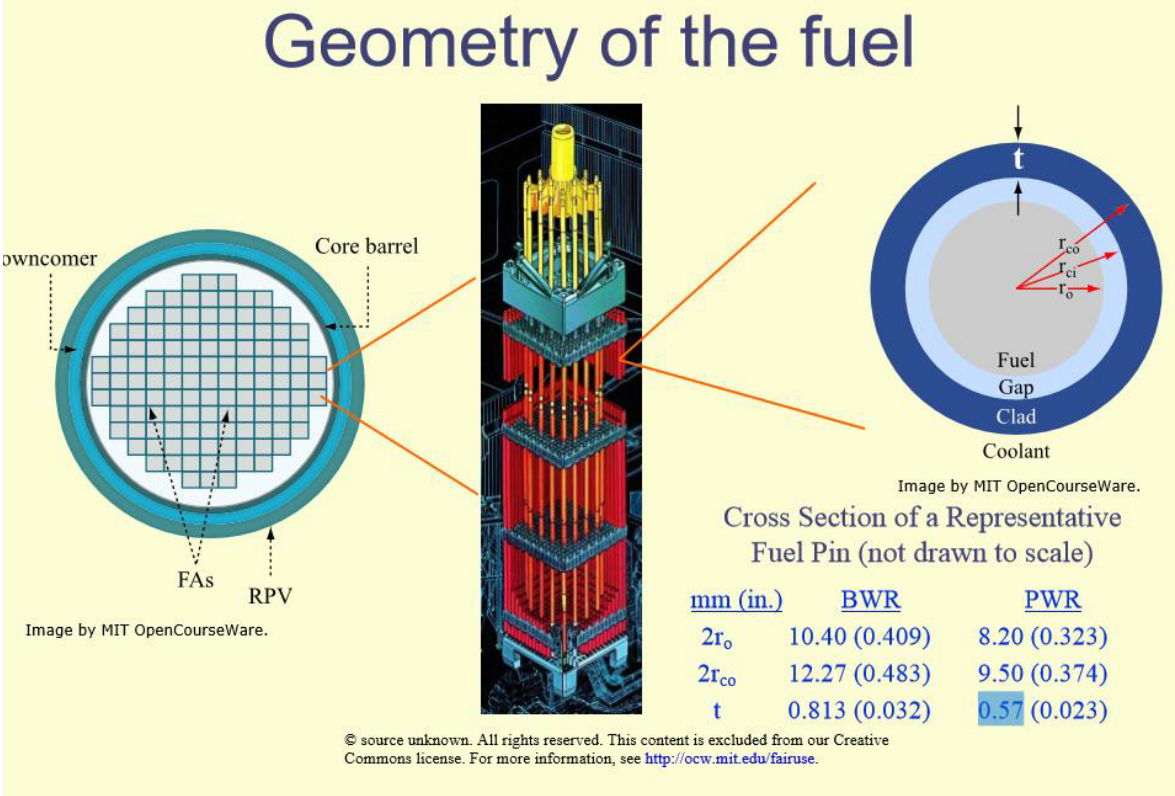

Figure 4-3 Geometry of fuel rods (from Buongiorno 2010).

The total weight of the fuel assembly is transferred to the horizontal plates at the interface between the plates and the spacer grids. It is assumed that the spacer grid width is 5 cm and the center-to-center spacing between the grids is 0.6 m. The fuel assembly characteristics are selected considering tables provided by Holtec (2018). Reference data for a 17×17 array configuration is presented in Table 4-1. The geometric details of the canister shell are listed in Table 4-2.

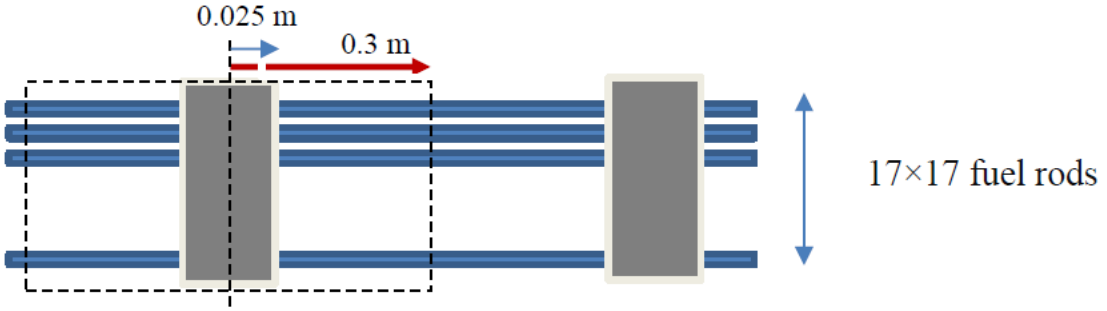

Figure 4-4 *FLAC3D* model representation along the canister axis (from SNL-ICG 2019). The black dotted box shows the extent of fuel assembly and spacer grid included in the model. Only half spacing between spacer grids shown by red arrow is represented in the *FLAC3D* model.

Table 4-1 PWR Fuel Assembly Characteristics (from Table 1.2.10, Holtec 2018)

Fuel Assembly Type	17×17A	17×17B	17×17C
Fuel Cladding Material	Zircaloy	Zircaloy	Zircaloy
# Fuel Pin Positions	264	264	264
Fuel Clad OD (in.)	≥ 0.360	≥ 0.372	≥ 0.377
Fuel Clad ID (in.)	≤ 0.3150	≤ 0.3310	≤ 0.3330
Fuel Pellet Dia. (in.)	≤ 0.3088	≤ 0.3232	≤ 0.3252
Fuel Rod Pitch (in.)	≥ 0.496	≥ 0.496	≥ 0.502
Active Fuel Length (in.)	≤ 150	≤ 150	≤ 150
# Guide and/or Instrument Tubes	25	25	25
Guide/Instrument Tube Wall Thickness (in.)	≥ 0.016	≥ 0.014	≥ 0.020

Table 4-2 Geometric Details of Canister (from Table 1.2.10, Holtec 2018)

Component	Inner Radius (in.)	Outer Radius (in.)	Height (in.)
Base Plate	0.	34.188	2.5
Canister Shell	33.688	34.188	178.0
Canister Lid	0.	34.188	9.5

Material Properties – It is assumed that the basket plates have the properties of aluminum. The Young's modulus, Poisson ratio and density are selected from Blue (2009) and are presented in Table 4-3. This source specifies a minimum tensile strength of 31.3 ksi (216 MPa) for the plates. For parts of this study that consider yielding of aluminum-based MMC basket plates, a slightly conservative tensile yield strength of 200 MPa will be used.

In the present modeling both the canister and the overpack are assumed to be made of stainless steel with identical properties. Holtec (2018) suggests that the canister is made from one of the "Alloy X" materials, and properties typical for stainless steel were used in the analysis. Values of Young's modulus, yield and ultimate strengths for stainless steels are reported by Holtec (2018). For this study we will use Young's modulus of 200 GPa, density of 8,031 kg/m^3, and Poisson ratio of 0.3 (at ambient temperature). For parts of the study that consider yielding of the DPC shell, a yield strength (and ultimate strength) of 445 MPa can be assumed for stainless steel at 200°C in a linearly elastic–perfectly plastic model.

Details of the fuel rods and spacer grids are not explicitly represented in the model because it would make the model prohibitively large and slow to execute. Both fuel rods and the spacer grids are represented using solid zones with equivalent stiffness and density, based on the Fuel/Basket Degradation model approach (SNL-ICG 2019). In these calculations, the density values of Zircaloy and uranium oxide were used to calculate the total weight of the fuel assembly and equivalent density of zones.

Table 4-3 Input Material Properties

Material	Young's Modulus (GPa)	Poisson Ratio	Density (kg/m^3)
Zircaloy			6,500
MMC (aluminum-based)	80	0.3	2,690
Uranium oxide pellets			10,970
Stainless steel	200	0.3	8,031

Model Description - It is expected that the dominant failure mode of the DPC will be controlled by buckling of the canister shell and the basket plates. Hence the initial modeling approach will be linear elastic, with failure occurring by buckling. Plate yielding can be evaluated if suggested by the buckling results. Results of a model of basket plate buckling under gravity due to plate thinning caused by corrosion are shown in Figure 4-5. In this model, the plates were represented as shell structural elements. However, the spacer grids and fuel assemblies inside the cells were represented as stiffer structural components that constrain deformation of the plates.

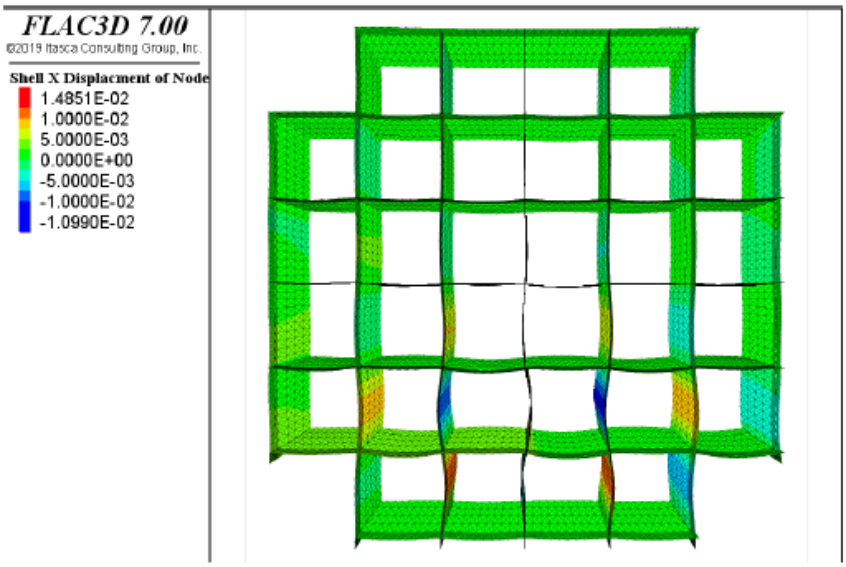

(a) onset of buckling

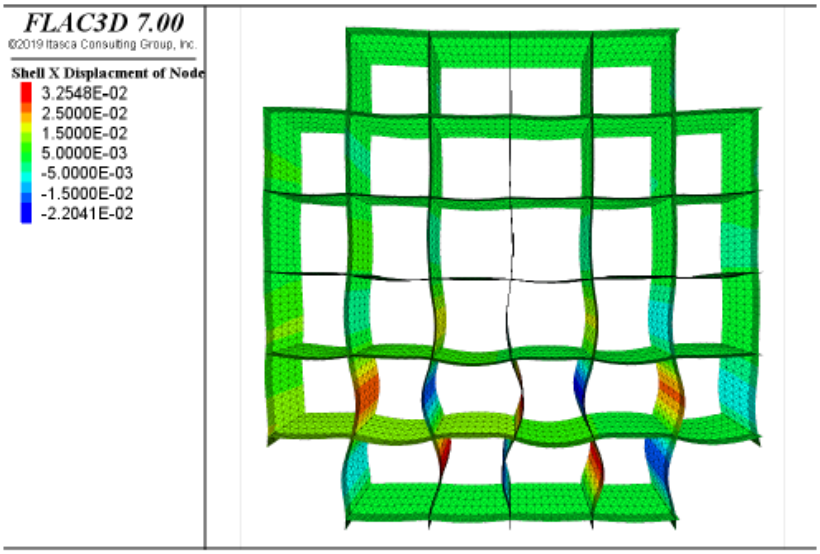

(b) a state during buckling

Figure 4-5 Deformation of the DPC basket due to buckling of the plates weakened by corrosion (Model B from SNL-ICG 2019, Figure 20).

The geometry of the DPC Crush Model in the cross-section is shown in Figure 4-6. The canister shell, support elements and the plates will be modeled as the shell structural elements. The shell elements used to represent the plates will have interfaces on both sides that will allow interaction between the plates and the fuel assembly. The fuel assembly will be represented using solid zones with the properties and geometry varying between sections that represent assembly of the fuel rods and the spacer grids.

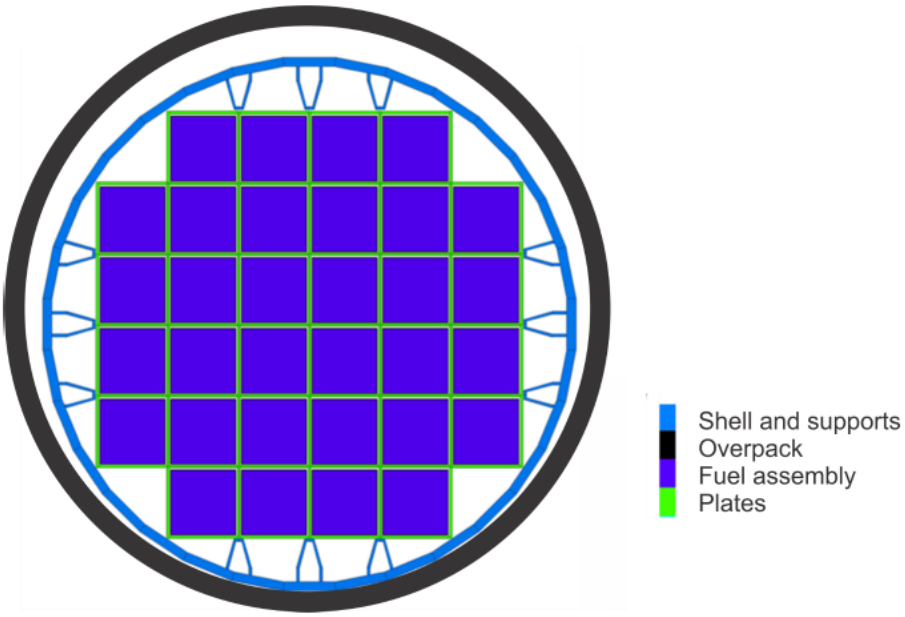

Figure 4-6 Geometry of the generic 32-PWR DPC model with egg-crate basket.

The horizontal and vertical plates will be slotted together such that in a given section (either vertical or horizontal) one plate is continuous while the other is cut (i.e., two sections can rotate independently). Each plate is 50% continuous and 50% cut.

4.2 Summary of Modeling Progress

The DPC Crush Model is being developed currently with preparation of this progress report, so model results are not yet available. Model results will be described in a planned FY21 summary deliverable.

5. Discussion

This section addresses the questions framed in the deliverable description (Section 1.4): 1) how fuel/basket damage, including from seismic ground motion, could impact reactivity; 2) whether dynamic degradation processes should be targets for further model development; and 3) identify key parameters and how they affect the likelihood and energy of criticality events.

5.1 Potential Reactivity Changes With Degraded Configurations

For a basket structure made from aluminum-based MMC material as analyzed in the Fuel/Basket Degradation Model (Section 2), basket collapse would coincide with loss of neutron absorbers. This means that considering the two degradation cases being used for reactivity modeling by Clarity et al. (2019) the basket degradation case is more meaningful than the loss-of-absorber case for aluminum-based MMC baskets.

Previous results from the Fuel Assembly Cell Model (SNL-ICG 2019) showed that absorber corrosion product redistribution and movement in response to ground motion could occur before basket collapse. Corrosion products containing grains of absorber material would accumulate in a layer at the bottom of each fuel assembly cell, assuming the package has been emplaced with the basket plates horizontal/vertical. (Emplacement of the waste package with the basket rotated at an angle to vertical would cause the corrosion products to accumulate in the corners of the fuel assembly cells.) Prior to basket collapse the neutron absorber density would become depleted on the vertical plates, which would cause reactivity to increase. This effect is bounded by the loss-of-absorber case (Clarity et al. 2019). In future work with stainless steel baskets, the loss-of-absorber case could possibly be modified to consider only depletion of vertical plates.

After collapse, the thinned basket plates will buckle, and the spacer grids will bear the weight of the fuel stack. Fuel pitch could be only slightly affected if the spacer grids are intact. Fuel reactivity may increase further at this point because fuel assemblies are brought into closer proximity and large voids may form due to rearrangement of assemblies, as shown by the Fuel/Basket Degradation Model. This condition corresponds approximately to the basket degradation case used by Clarity et al. (2019), but representative voided configurations may be more reactive.

Basket collapse is an important transition when fuel weight loads are transferred from the basket to the spacer grids. Timing of this transition depends on the rates of corrosion, basket configuration, and modes of deformation. For the egg-crate type basket analyzed in this work, collapse failure can occur due to buckling of aluminum-based MMC plates, or possibly by hinge-type failures at the joints between plates which have not yet been analyzed (see Section 6.1). Tube-and-plate basket configurations made mostly from stainless steels have also not yet been analyzed (Section 6.1).

Basket structure made from stainless steel may not collapse during the period of regulatory concern. The corrosion lifetime of stainless steel could be far greater than the 25,000 years assumed by Jerden et al. (2017) if the retreat rate of the corrosion front is less than 0.1 μm per year (1 μm per year is assumed for discussion in Section 2.1). The smaller rate is plausible for stainless steel in benign chemical environments (no added chloride, oxic conditions) and low ambient temperature typical of repository conditions after the first few thousands of years (Kursten et al. 2004, discussed by Ilgen et al. 2014). For anoxic conditions corrosion rates are reported to be even smaller (0.001 to 0.1 μm per year). Use of these results could extend the mechanical lifetime for stainless steel basket structures to well beyond 100,000 years, thereby simplifying reactivity

modeling for as-loaded DPCs. Note that this is for general corrosion, which is relevant if localized corrosion (cracking, pitting) is not the cause of basket collapse (see Section 6.1).

Further degradation beyond basket collapse would involve failure of Zircaloy spacer grids and fuel rod cladding. Section 2 includes preliminary examples of successive grid failures simulated using the 2.5-D model, and a resulting sequence of degraded states (Figures 2-8 through 2-10).

Basket plate degradation and collapse could produce voids in the fuel stack that are not represented in the degraded basket case used for reactivity analysis (Clarity et al. 2019). In other words, path dependence of basket degradation could produce intermediate states that are more reactive than the final state.

Degraded configuration beyond basket collapse has not been addressed in the degradation cases for reactivity analysis (Clarity et al. 2019). However, the calculated examples (Figures 2-8 through 2-10) show that further voiding of the fuel stack could occur from selective collapse of spacer grids. Rapid increase of reactivity could also occur from voiding by spacer grid collapse during seismic ground motion (which has not yet been analyzed). The importance of seismic events could increase with time in tectonically active geologic settings, as the seismic hazard increases with the duration of exposure following basket collapse. Spacer grids could last for many thousands of years after waste package breach, while basket collapse could occur after only a few hundred years, for baskets made from aluminum-based materials. Accordingly, future work should analyze potential reconfiguration by seismic ground motion.

Total collapse of the fuel in a DPC would be caused by degradation of the basket plates and failure of the spacer grids, possibly with degradation of fuel rods as well. The result would be a disorganized slump structure with smaller effective pitch between fuel rods, and corrosion products (less hydrogen density than free water) filling interstices between fuel rods. Degradation of basket structure and spacer grids could ultimately terminate any type of postclosure criticality by decreasing the effective pitch of fuel rods and decreasing the interstitial moderator density. If the fuel cladding also degrades, additional complications may result from transport of fissiles and solubilization of absorber isotopes in the fuel (Alsaed 2020). Hence it is important to understand the relative corrosion rates of spacer grids and fuel rods, once the basket structure has collapsed. This discussion affirms that intermediate states of degradation could be more reactive than final degraded states.

Dynamic responses to ground motion could cause rapid voiding of fuel assemblies and redistribution of neutron absorber materials, leading to transient criticality events. Previous work analyzed a damaged state caused by ground motion, in which basket plates were failed and fuel assemblies were shifted but remained in stacks, with increased void spaces between them (SNL-ICG 2019, Figure 38). Results reported in Section 2 (Figures 2-7 through 2-9) suggest that rapid voiding may also occur from dynamic failure of spacer grids. The importance of ground motion to reactivity changes from rapid voiding behavior, with and without basket plates, has not yet been analyzed.

The Fuel/Basket Degradation Model (Section 2) showed that PWR assembly guide tubes (representing disposal control rods) move with the fuel rods during degradation, as expected. Further reactivity analysis of degraded states (forthcoming deliverable M3SF-20OR0103050126) will be helpful for specifying the number and distribution of disposal control rods, re-channeled BWR fuel assemblies, and chevron inserts, and for designing calculation strategies to verify subcriticality for degraded DPC fuel and baskets.

5.2 Waste Package Breach Model Constraints on Transient Criticality Events

A minimum thermal event energy was found to be necessary for fracture growth or yielding of the canister (approximately 0.2 GJ). At lower event energy the heat would be absorbed into the canister internals, including water, without producing sufficient pressure to open a fracture or yield the canister shell.

Under the assumptions of the model (Section 3) the fracture always opens and grows when a critical pressure is reached. Successive events increase the fracture length, which increases stress concentration around the fracture tips and allows the fracture to open and expel fluid at lower pressures.

Trial model solutions (Figure 3-8) suggest there is an energy level greater than 1 GJ and less than 10 GJ at which boiling may occur. The specific conditions for boiling are likely to depend on the rate of heating, localization of heating inside the canister, and the transmissivity of the vessel breach. The maximum differential pressure that can be sustained by a waste package is approximately 15 MPa with the wall thickness values evaluated, at which point vessel rupture occurs.

Under the model assumptions the canister always returns to its original dimensions and the fracture closes, at the end of each event. If permanent non-reversible deformation of the canister were included, the fracture could acquire a permanent opening aperture. This could further lower the pressure that could be achieved by subsequent events, which in turn could lower the energy of subsequent criticality excursions. To verify how fracture opening and growth could affect criticality event dynamics and total energy, requires close-coupling with a neutronic model (Stage IV in Section 1).

6. Summary and Recommendations

6.1 Summary and Recommendations for the Fuel/Basket Degradation Model

The following tasks have been completed for the basket degradation model:

- The model has been ported from *3DEC* 5.2 to *PFC* 6.0. A shorter 2.5-D model has also been set up to relatively quickly test new features and gain insight into model behavior.
- The *softbond* lumped constitutive model for contacts in *PFC* has been modified to simulate the bilinear moment-curvature response of fuel rods observed in the lab and is currently being tested.
- Some trial simulations have been run using the 2.5-D model, including simulating the degradation of basket plates followed by progressive degradation of spacer grids under the greatest load.

Using the model, degraded states have been simulated for degradation of all basket plates, thereby verifying the loss-of-absorber and basket-degradation cases used in reactivity analysis. Additional voiding caused by rearrangement of fuel assemblies may further increase reactivity, more than the degraded basket case.

Subsequent degradation of spacer grids may produce additional voiding that could increase reactivity beyond the cases used in reactivity analysis. The timing of basket plate degradation varies between rapid (for aluminum-based plates) and slow (for stainless steel). For many disposal environments (no added chloride, neutral to alkaline pH, temperature cooled to ambient) stainless steel corrosion could be slow enough that the mechanical lifetime of basket plates is more than 100,000 years.

Degraded states can be simulated using relative corrosion rates, to show how criticality control features (e.g., disposal control rods; SNL 2020) move with the fuel rods (Stage III).

Coupling of the Fuel/Basket Degradation Model with neutronics and thermal-hydraulics will initially be external, by providing degraded configurations for reactivity analysis (Stage II in Section 1). Later coupling could also be external, but two-way so that criticality event energy can change the state of the canister/overpack (Stage IV).

Sensitivity analyses are needed to study the effects of uncertainty in the timing of degradation steps, which can be implemented as randomness in the effective rates of strength degradation for different components. For example, corrosion rates for basket plates may be nonuniform and heterogenous, so that certain sections of the basket degrade faster than others. The same idea can be applied to the internal supports between the shell and basket. Heterogeneity can be implemented by failing only a fraction of structural components completely (e.g., degradation of 50% of the spacer grids).

The following features are planned to be implemented in the additional runs of the Fuel/Basket Degradation Model as implemented in the *PFC* code:

- Include the modified *softbond PFC* model feature to capture bilinear moment-curvature response of fuel rods.
- Improve the discretization for spacer grids and add the hinge formation model.
- Include the disposal overpack in the model.

- Test additional scenarios, including failure of internal supports in the canister and of the canister.

These results are planned to be described in a FY21 summary deliverable.

Other topics that can be explored in future work (FY21 or beyond) include:

- Test the 3-D model for additional modes of deformation, failure, rearrangement, and voiding.
- Simulate spacer grid collapse due to seismic ground motion.
- Simulate tube-and-plate basket structure degradation, which would involve basket components made from stainless steel.
- Evaluate the mechanical lifetime for stainless steel basket structures, potentially providing justification for not using the basket degradation case for reactivity analysis (if the basket mechanical lifetime is on the order of 100,000 years or longer). Take into account modes of corrosion (e.g., general corrosion vs. localized cracking), kinematics of degradation, and modes of basket failure such as hinge failure at the joints between plates.
- Incorporate criticality control features (SNL 2020) that could be added to DPCs loaded in the future, particularly BWR fuel assembly channels made from advanced neutron absorbing material, and chevron insert plates (Stage III in Section 1).

6.2 Summary and Recommendations for the Waste Package Breach Model

Progress in development of the Waste Package Breach Model is summarized in Figures 3-8 through 3-10. Processes added to the model (in addition to fracture growth and canister yield) include: a zero-dimensional thermal-hydraulic model, heat pulse input, fracture opening/growth or canister yielding, venting of fluid pressure, and dissipation of pressure outside the waste package. Multiple successive heating events were simulated (subject to limitations listed below).

Limitations of the current model include the following, some of which will be addressed in planned work as indicated:

- The model is currently implemented for single phase liquid water only, and two-phase non-isothermal flow will be included in planned work.
- Coupling of the backfill pore pressure (external to the waste package) with the thermal-hydraulic model is approximate and may underestimate mass flow during early times in the case of fast loading, because steady-state flow conditions are assumed to be reached instantaneously for the backfill. In addition, conductive dissipation of heat from the waste package is not included. These limitations will be addressed in planned work.
- The vessel mechanical response to pressurization is quasi-static and neglects dynamic effects. Coupling the quasi-static response to the time-dependent thermal-hydraulic model may overpredict the rate of deformation during fast loading. (The effect on flow venting tends to counteract the underprediction of flow described in the previous bullet.) Inertial effects on fracture opening can be investigated using *FLAC3D*.
- The mechanical model assumes a linearly elastic, perfectly plastic material behavior. It is known that the mechanical response of steel is nonlinear in the failure region.

- The zero-dimensional approximation is applicable for times more than about 0.5 msec after event initiation. Realistic criticality events on such a short timescale may be localized in a small region inside the canister. Spatial gradients in pressure and temperature may exist for short times, and local boiling may occur in the area of the criticality. The model presented in this work transfers heat instantaneously, and as a result the heat is spread which prevents boiling for the magnitude of heating events studied. Despite this, the vessel response to pressure is realistic because a fracture would actually respond mechanically to the average internal pressure over the timescale of interest.
- The model currently represents mass flow outward from the package, but does not account for cooling of the package and return flow. This enhancement would include cooling of the waste package by outward dissipation of heat, followed by pressure dissipation and return flow through breaches. Dissipation processes and return flow are needed along with two-phase water-steam behavior for future coupling with neutronic/thermal-hydraulic models to represent more energetic transient events.

The mechanical response curves described in Section 3.3.1 are valid for a given starting fracture length and for monotonically increasing pressure. Whereas they are used to describe the unloading and reloading behavior, they do not take into account permanent fracture deformation. There is a size effect on the pressure required to grow the fracture; longer fractures open and grow at lower pressures because the stress concentration is higher. This will be addressed in future work by running the mechanical model for different initial fracture lengths, which will improve the accuracy of the model for predicting the behavior of repeated events.

Despite these qualifiers, the modeling approach presented in this work has these attributes:

- The model captures the key physical processes.
- Run time is fast.
- The formulation is straightforward and readily explained.
- The model is ready for use in probabilistic analysis or parametric studies.
- The model is anticipated to be mature enough in the foreseeable future for integration with closely coupled neutronic/thermal-hydraulic models (Stage IV in Section 1).

Additional results will be described in a planned FY21 summary deliverable.

References

Ahn, T., H. Akhavannik, G. Bjorkman, F.C. Chang, W. Reed, A. Rigato, D. Tang, R.D. Torres, B.H. White and V. Wilson 2018. *Dry Storage and Transportation of High Burnup Spent Nuclear Fuel*. NUREG-2224. Office of Nuclear Material Safety and Safeguards, U.S. Nuclear Regulatory Commission.

Alsaed, A. 2020. *Permanent Criticality Termination Processes in Disposed DPCs.* M4SF-20SN010305063 (SAND2020-6615 R). U.S. Department of Energy, Office of Spent Fuel and Waste Science and Technology.

Blue, P. 2009. *Material Qualification Program for Metamic-HT for use in HI-Star 180 Fuel Basket*. Holtec International.

Bowles, J.E. 1997. *Foundation Analysis and Design*. Fifth Edition. The McGraw-Hill Companies, Inc.

BSC (Bechtel-SAIC Co.) 2004. *Development of Earthquake Ground Motion Input for Preclosure Seismic Design and Postclosure Performance Assessment for a Geologic Repository at Yucca Mountain, NV*. MDL-MGR-GS-000003 Rev. 1. U.S. Department of Energy, Office of Civilian Radioactive Waste Management. November, 2004.

Buongiorno, J. 2010. *PWR Description*. Center for Advance Nuclear Energy Systems, Massachusetts Institute of Technology. (https://ocw.mit.edu/courses/nuclear-engineering/22-06-engineering-of-nuclear-systems-fall-2010/lectures-and-readings/MIT22_06F10_lec06a.pdf)

Clarity, J.B., K. Banerjee and L.P. Miller 2019. *Canister Reactivity and Ground water Absorption Analyses*. M3SF-19OR010305013. U.S. Department of Energy, Office of Spent Fuel and Waste Science and Technology.

Davidson, G.G., M. Swinney, S. Johnson, S. Bhatt and K. Banerjee 2019. *Initial Neutronics and Thermal-Hydraulic Coupling for Spent Nuclear Fuel Canister*. M3SF-19OR010305015. U.S. Department of Energy, Office of Spent Fuel and Waste Science and Technology.

Holtec (Holtec International) 2018. *Safety Analysis Report on the HI-STAR 100 MB Package, Version 0, Revision 15*. Issued October 11, 2010.

Ilgen, A., C. Bryan, S. Teich-McGoldrick, E. Hardin and J. Clarity 2014. *DPC Materials and Corrosion Environments*. FCRD-UFD-2014-000597. U.S. Department of Energy, Office of Used Nuclear Fuel Disposition. September, 2014.

IAPWS (International Association for the Properties of Water and Steam) 2018. "Revised Release on the IAPWS Formulation 1995 for the Thermodynamic Properties of Ordinary Water Substance for General and Scientific Use." Ref. R6-95. (http://www.iapws.org/relguide/IAPWS-95.html)

Itasca (Itasca Consulting Group, Inc.) 2016. *3DEC — Distinct-element Modeling of Jointed and Blocky Material in 3D, Ver 5.2*. Minneapolis: Itasca.

Itasca (Itasca Consulting Group, Inc.) 2018. *PFC — General Purpose Distinct-Element Modeling Framework, Ver 6.0*. Minneapolis: Itasca.

Itasca (Itasca Consulting Group, Inc.) 2019. *FLAC3D — Fast Lagrangian Analysis of Continua in Three-Dimensions, Ver. 7.0*. Minneapolis, Minnesota.

Jerden, J., K. Frey and W. Ebert 2017. *Spent Fuel Matrix Degradation and Canister Corrosion: Quantifying the Effect of Hydrogen*. SFWD-SFWST-2017-000039 and SFWD-SFWST-2017-000042. U.S. Department of Energy, Office of Spent Fuel and Waste Science and Technology.

Kursten, B., E. Smailos, I. Azkarate, L. Werme, N.R. Smart and G. Santarini 2004. *COBECOMA: State-of-the-art document on the COrrosion BEhaviour of COntainer MAterials.* European Commission 5th Euratom Framework Programme, 1998-2002. Contract # FIKW-CT-20014-20138 Final Report: European Commission.

Lee, S.-H., J. Kim and K. Song 2007. "Design improvement of an OPT-H type nuclear fuel rod support grid by using an axiomatic design and an optimization." *Journal of Mechanical Science and Technology*. 21, 1191-1195 (10.1007/BF03179035).

McLaughlin, T.P., S.P Monahan, N.L. Pruvost, V.V. Frolov, B.G. Ryazanov and V.I. Sviridov 2000. *A Review of Criticality Accidents, 2000 Revision.* LA-13638. Los Alamos National Laboratory.

Price, L.L., A.A. Alsaed, A. Barela, P.V. Brady, F. Gelbard, M.B. Gross, M. Nole, J.L. Prouty, K. Banerjee, G.G. Davidson, Z. Fang, S. Painter and M. Swinney 2019. *Preliminary Analysis of Postclosure DPC Criticality Consequences*. M3SF-19SN010305062. U.S. Department of Energy, Office of Spent Fuel and Waste Science and Technology. December 2019.

SNL (Sandia National Laboratories) 2020. *Options for Future Fuel/Basket Modifications for DPC Disposition*. M4SF-20SN010305051, Rev. 1. U.S. Department of Energy, Office of Spent Fuel and Waste Science & Technology. June 2020.

SNL-ICG (Sandia National Laboratories and Itasca Consulting Group) 2019. *DPC Criticality Simulation Preliminary Phase: Fuel/Basket Degradation Models*. M3SF-19SN010305071. U.S. Department of Energy, Office of Spent Fuel and Waste Science and Technology. September 2019.